Science of the Total Environment 733 (2020) 139193

Contents lists available at ScienceDirect

Science of the Total Environment

journal homepage: www.elsevier.com/locate/scitotenv

# Effects of natural light and depth on rates of photo-oxidation of dissolved organic carbon in a major black-water river, the Rio Negro, Brazil

Ora E. Johannsson [a,*], Marcio S. Ferreira [b], D. Scott Smith [c], Anne Crémazy [a,d], Chris M. Wood [a,b], Adalberto L. Val [b]

[a] Department of Zoology, University of British Columbia, Vancouver, BC V6T 1Z4, Canada
[b] Laboratory of Ecophysiology and Molecular Evolution, Brazilian National Institute for Research of the Amazon, INPA, Manaus, AM, Brazil
[c] Department of Chemistry and Biochemistry, Wilfrid Laurier University, Waterloo, ON N2L 3C5, Canada
[d] Biological Sciences, University of New Brunswick, Saint John, NB E2L 4L5, Canada

## HIGHLIGHTS

- Photo-oxidation of DOC returns $CO_2$ to the atmosphere, importance in tropical rivers?
- Surface photo-oxidation was high (0.80–0.86 mg C $l^{-1}$): areal, 28.8–39.3 mg C $m^{-2}$ $d^{-1}$
- Light controls rate of photo-oxidation through seasonal cycle from dry to wet season
- Complete photo-oxidation and absorbance losses extend to a maximum of 15 cm
- Partial photo-oxidation, seen as fluorescence losses, extends to 35–43 cm depth

## GRAPHICAL ABSTRACT

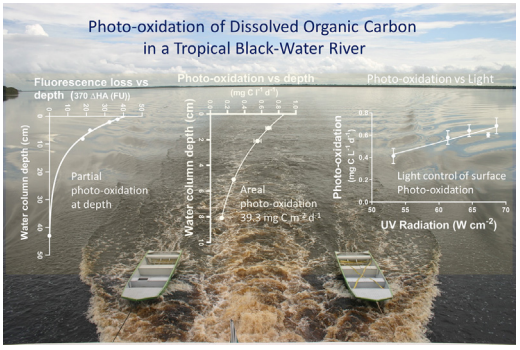


## ARTICLE INFO

*Article history:*
Received 28 January 2020
Received in revised form 9 April 2020
Accepted 1 May 2020
Available online 8 May 2020

Editor: Sergi Sabater

*Keywords:*
DOC
PARAFAC
Fluorescence
Absorbance
Partial photo-oxidation

## ABSTRACT

Systems rich in terrigenous dissolved organic carbon (DOC), like the Rio Negro, can contribute significant amounts of carbon dioxide back to the atmosphere and support important microbial communities. We investigated photo-oxidation in the Rio Negro: (1) the depth to which light causes complete photo-oxidation to $CO_2$ and changes in DOC structure, (2) the daily rate of change of absorbance indices, (3) the relationship between sub-surface rates of photo-oxidation to $CO_2$ and light exposure, (4) the areal rates of photo-oxidation, and (5) the stability of fluorophore signals. Experiments were run in an outdoor pool of Rio Negro water, under natural sunlight during the dry seasons of 2015 and 2018. In 2018, rates of complete photo-oxidation and changes in absorbance indices decayed exponentially, approaching their asymptotes between 9 and 15 cm depth. In 2015, direct absorbance indices ceased changing at 14 cm depth. Fluorescence of humic acid-like moieties continued to decrease, sometimes to 35–43 cm depth. This indicates that partial photo-oxidation of DOC, and thus interaction with the microbial community, occurs to greater depths than previously expected. Areal rates of $CO_2$ production were 28.8 and 39.3 mg C $m^{-2}$ $d^{-1}$ (two experiments, October 2018). Sub-surface (1.1 cm) rates were strongly related to light levels, reaching a maximum of 0.68 mg C $l^{-1}$ $d^{-1}$ in September. Complete photo-oxidation ceased below 29.6 mW $cm^{-2}$ $d^{-1}$ UV radiation, providing a daily baseline for observable production of $CO_2$. Absorbance indices changed by 9 to 14% $d^{-1}$ at high light levels, except for $R_{254/365}$ (4.4% $d^{-1}$).

*Abbreviations:* UV-R, UVA + UVB radiation; $\Delta Index_{(d=1)}$, change in an absorbance or fluorescence index over the first day of radiation; λ, wavelength of light (nm); $\mu_{(\lambda)}$, linear attenuation co-efficient of wavelength λ ($cm^{-2}$); $Abs_{(\lambda)}$, absorbance of light wavelength λ over a distance of 1 cm; d, depth of penetration of λ into a water column (cm); dp, depth down into the water column (cm); K, rate of change per unit of x-axis in exponential equation.

* Corresponding author.
*E-mail address:* johannss@zoology.ubc.ca (O.E. Johannsson).

https://doi.org/10.1016/j.scitotenv.2020.139193

Fluorophore emission ranges were stable between 2014 and 2018, indicating that emissions can be compared across time and space. This study contributes to better estimates and understanding of photo-oxidation in tropical, black-water rivers, which will be useful for carbon modelling.



## 1. Introduction

Returning carbon from aquatic systems to the atmosphere as $CO_2$ is a globally important carbon pathway (Cole et al., 2007; Koehler et al., 2014). Cole et al. (2007) estimated that approximately 50% of carbon entering freshwater systems is returned to the atmosphere as $CO_2$. Raymond et al. (2013) calculated that roughly 2.1 petagrams of carbon are returned to the atmosphere from freshwater systems each year – 18% from lakes and reservoirs, the remaining 82% from rivers and streams. Photo-oxidation of dissolved organic carbon (DOC) contributes to this $CO_2$ evasion. Koehler et al. (2014) calculated that roughly 10% of all $CO_2$ released back to the atmosphere from lakes and reservoirs was through photo-oxidation of DOC. A similar estimate has not yet been derived for rivers and streams.

Aquatic systems with shorter residence times, like many rivers, have more rapid photo-oxidation of DOC and production of $CO_2$ than deeper more static systems, due to their greater relative exposure of DOC to light and fresher sources of DOC (Molot and Dillon, 1997; Porcal et al., 2013a). Much of the photo-oxidation of terrestrially-derived DOC starts in rivers (Cory et al., 2014; Porcal et al., 2013a). Thus, rivers, streams and shallow water bodies with rapid turnover could also be important in returning $CO_2$ to the atmosphere through photo-oxidation (Molot and Dillon, 1997; Cory et al., 2014; Lapierre and del Giorgio, 2014; Evans et al., 2017). In tropical regions, such as the Amazon, rivers, streams and flooded forest are the dominant aquatic systems. For this reason, we are interested in the extent and control of photo-oxidation in the Rio Negro (Brazil) as an example of such processes in large forested, tropical, black-water rivers.

The black waters of the Amazon Basin are DOC-rich systems (Thurman, 1985). The great lengths of these rivers mean that the area and amount of time for photo-oxidation are relatively large. In addition, the warm temperatures and relatively low pH of these rivers and intense sunlight of the tropics can favour higher rates of photo-oxidation (Molot and Dillon, 1997; Granéli et al., 1998; Anesio and Granéli, 2003; Porcal et al., 2015). Photo-oxidation of DOC in the Rio Negro is of particular interest due to the large size of the river (the Rio Negro is over 2000 km long with a discharge of 29,000 $m^3\ s^{-1}$ (Ertel et al., 1986; Latrubesse and Franzinelle, 2005)), the high levels of $CO_2$ off-gassing observed from the river (Richey et al., 2002) and the importance of DOC in structuring and supporting a biologically diverse and economically important ecosystem (Val and Almeida Val, 1995; Alho et al., 2015; Beltrão et al., 2019).

The DOC of the Rio Negro has been characterized as particularly high in humic substances (70%) with a low fulvic acid to humic acid ratio (Thurman, 1985; Ertel et al., 1986). Such DOC is primarily derived from forests and is more recalcitrant to biological degradation (Lapierre and del Giorgio, 2014). Amon and Benner (1996a) found that the rate of photo-oxidation of this DOC was 7× greater than the rate of bacterial DOC consumption. Rates of photo-oxidation of Rio Negro DOC have been measured on several occasions, with estimates of near-surface $CO_2$ production ranging from 0.45 to 1.17 mg C $l^{-1}\ d^{-1}$ (Amon and Benner, 1996a; Granéli et al., 1998; Johannsson et al., 2017). However, the rates were not related to environmental conditions. Each was a measurement in time. None of the rates were normalized to DOC concentration (DOC was not always measured), and methods varied. Only one study has estimated areal production (Remmington et al., 2011: 24 mg C $m^{-2}\ d^{-1}$, just upstream of Manaus): the authors consider the estimate to be very conservative.

The environmental and chemical factors governing rates of photo-oxidation are locally variable, thus understanding needs to start with local knowledge. Much is known about the relationships of photo-oxidation with light intensity (Vähätalo et al., 2000; Porcal et al., 2013b) and the light spectrum (Granéli et al., 1998). However, water transparency which is site- and time- specific, will modify the light environment experienced by DOC. The Rio Negro is an iron-rich river; therefore, the low pH is expected to increase the rate of photo-oxidative processes (Küchler and Forsberg, 2000; Molot et al., 2005). Less is known about the relationships between photo-oxidation and oxygen concentration and higher temperatures (>25 °C) (Anesio and Granéli, 2003; Patel-Sorrentino et al., 2004; Molot et al., 2005; Porcal et al., 2015).

In order to develop predictive models of photo-oxidation, a number of relationships need to be determined. These include the maximum depth at which light penetration no longer results in complete or partial photo-oxidation as well as the relationship between a simple measure of light intensity and the rate of photo-oxidation. Effects of environmental conditions such as temperature, oxygen and pH, on rates of photo-oxidation are also required. Some of this information is known, but not completely or not for tropical systems. The 'quality' of the DOC – its previous degradation history and degree of recalcitrance – will also affect the degree of photo-oxidation. The present study focused on the Rio Negro and aimed to understand the overall controls on DOC photo-oxidation with the secondary view towards developing predictive models. The specific goals were:

(1) to determine the depths at which light ceased to cause measurable photo-oxidative changes in the DOC and to determine how DOC responses were related to measures of surface UV radiation, temperature and water transparency,
(2) to provide normalized rates of loss of DOC and of absorbance indices, and
(3) to determine the rate of photo-oxidation near the surface and its relationship with UV light energy measured just above the water surface,
(4) to determine areal rates of photo-oxidative $CO_2$ production,
(5) to develop fluorescence metrics for Rio Negro DOC to allow comparison of fluorophores across time and space.

## 2. Methods

Photo-oxidation studies were undertaken during the dry season at the Instituto Nacional de Pesquisas da Amazônia (INPA) in Manaus, Brazil in mid-November-mid-December 2015 and in mid-September-mid-October 2018. December is considered the start of the wet season.

### 2.1. Offshore water collection

Experimental water was collected offshore approximately 30 km upstream from Manaus off of Praia do Açutuba (3° 04′ 17.7″S, 60° 20′ 26.7 W) on November 14th 2015 and September 20th 2018 (Fig. 1). Acid-cleaned, ultrapure water-rinsed carboys were submerged and filled with water from approximately 10 cm depth. The carbouys were brought back to INPA and stored at ≤4 °C. The experimental water was filtered within two days through a 0.45-μm filter (polyethersulfone filter, Membrane Solution, Dallas, TX, USA in 2015, or a cellulose-acetate filter, Fisher Scientific, Ottawa, ON, Canada, in 2018). It was returned

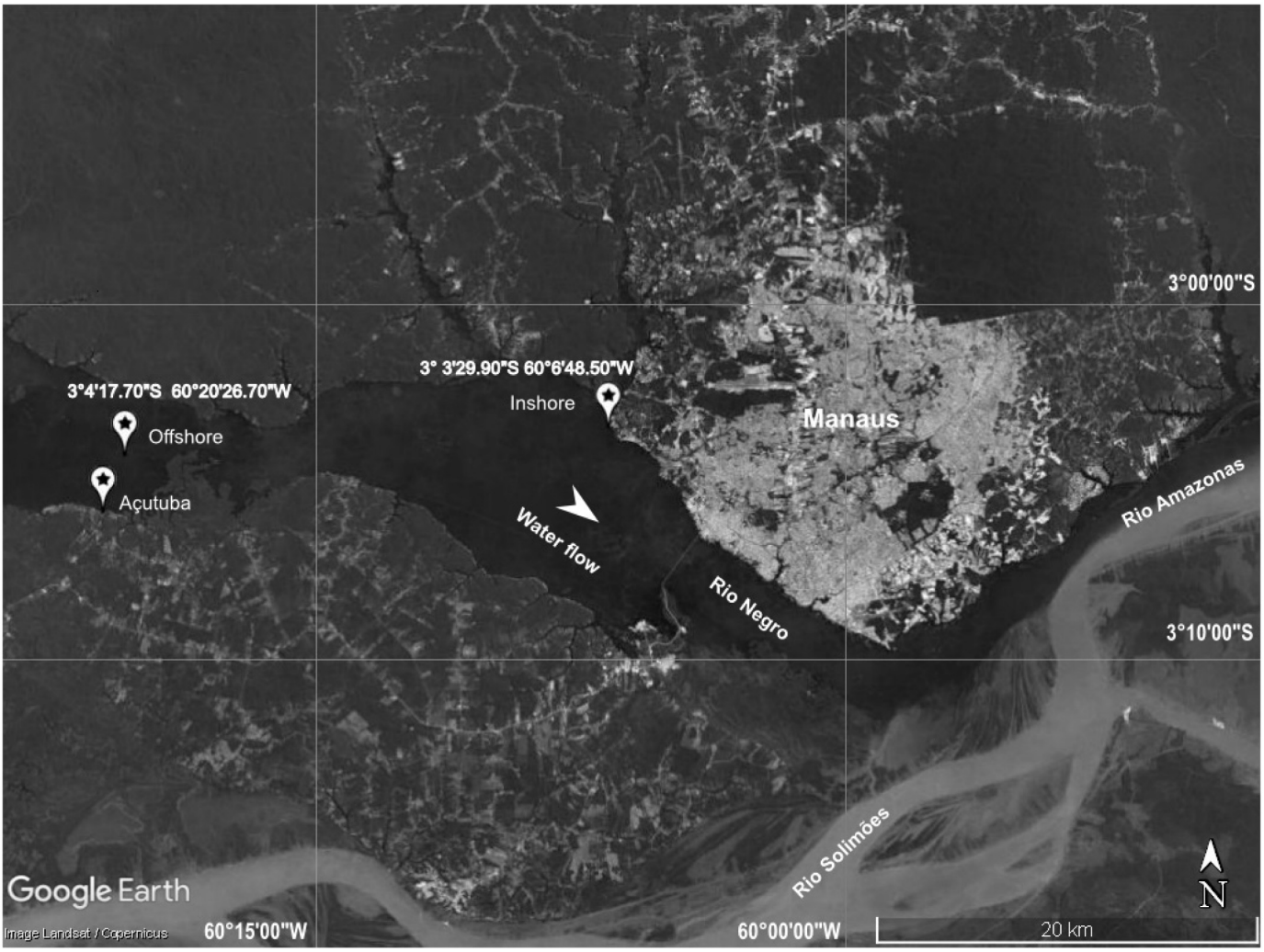


**Fig. 1.** Map of the Rio Negro River, Amazonas, Brazil, in the vicinity of Manaus. Experimental water was collected at the offshore of Praia do Açutuba (3° 04′ 17.7″S, 60° 20′ 26.7″W). Water for the pool was collected upstream of Manaus at the nearshore site (3° 03′ 29.9″S).

to storage at ≤4 °C, and used within the next 28 days. Ultrapure water was obtained from a Milli-Q Integral 5 Water Purification System (MilliporeSigma, Merck KGaA, Darmstadt, Germany). All containers used in the experiments were acid-washed and ultrapure water rinsed.

### 2.2. Experimental setup

Experiments were run under as natural conditions as possible. A plastic outdoor pool [150 cm × 205 cm × 50 cm depth] was filled with 1200 l of nearshore Rio Negro water. The pool water had been collected from off a dock upstream of Manaus (3° 03′ 29.9″S, 60° 06′ 48.5″W) (Fig. 1) and siphoned into the pool the same afternoon. The pool was covered by a tent when experiments were not running in order to protect the DOC from photo-oxidation. During experiments, the pool was covered by a tent during rain events and overnight due to possible rain events at night. It was removed between 8:00 a.m. and 8:30 a.m. The pool received uninterrupted sunlight from 8:30 a.m. until 3:30 p.m. and light shade from 3:30 p.m. until 6:00 p.m. The water was changed every two weeks to maintain natural absorbance characteristics. Adjustable metal racks were suspended in the water. The depths of the racks, relative to the water's surface, could be set at the beginning of each experiment and maintained at this depth using ground water to counter evaporative losses. The ground water was virtually devoid of DOC and colour (DOC = 0.34 mg $l^{-1}$, Crémazy et al., 2016). Temperature fluctuated diurnally in the pool. A chiller limited pool temperature fluctuations to 28.2–33.5 °C in 2015 and 28.6–35.8 °C in 2018. River surface water can reach temperatures of at least 34.5 °C by mid-day (O.E. Johannsson, M.S. Ferreira, C.M. Wood and A.L. Val, unpublished data). The pool water was well circulated with submersible pumps maintaining homogeneous temperatures throughout.

Two types of experimental containers were used: (1) 120-ml, flint-quartz bottles, 5-cm in diameter which were sealed with a film of saran wrap under a screw-top lid (2015) (saran wrap, S.C. Johnson & Son, Inc., Brantford, Canada), and (2) 1.8-cm diameter, 35-ml, quartz tubes which were sealed with silicone stoppers and Parafilm (2018) (Parafilm, Amcor Corporate, Zürich, Switzerland). Flint-quartz and quartz differ in their transparency to light. Quartz lets through ≥92% of all UV radiation (http://www.technicalglass.com/fused_quartz_transmission.html), while flint-quartz only transmits wavelengths longer than 350 nm at >80% transmittance (Fig. 12 of Dias et al., 2010). The flint-quartz data are included because they corroborate a number of the 2018 findings and provided information on light conditions at a different time of year. Additionally, comparisons between the two data sets indicated the relative importance of the lower wavelengths to photo-oxidation.

When setting up the experiments, the filtered, offshore Rio Negro water was poured into Nalgene containers and warmed to room temperature – 25–27 °C (Nalgene, Nalge Nunc International Corporation, Rochester, NY 14625, USA). The water was continuously mixed on a stir plate. The oxygen concentration was measured with an YSI 550A-

12 portable oxygen probe and meter (YSI INC., Yellow Springs, OH, USA). Each experimental flint-quartz or quartz container was filled to overflowing by siphoning water from the Nalgene container, keeping the inflow well below the water level to avoid changing the oxygen content. The containers were sealed without bubbles. They were placed in the pool early in the morning and retrieved at the same time of day two to four days later, depending on the amount of sun exposure. Each experiment consisted of initial, light-exposed and dark-control samples. Initial samples were collected when the experiment was set up to record initial conditions. Light-exposed samples were exposed to sunlight during the experiment and dark-control samples were wrapped in aluminum foil and placed in the pool in parallel with the light-exposed samples.

### 2.3. Experiments

A series of 9 experiments were run over the two field seasons. The experimental designs and physical conditions of each experiment are presented in Table 1. Changes in absorbance and fluorescence losses with depth were investigated in experiments 1–4 (2015 – flint quartz bottles) and experiments 7 and 8 (2018 - quartz tubes) (goal 1). Experiments 1 and 2 delimited the depth range of detectible absorbance losses. Experiments 4 and 8 ran bottles at 4 depths within that range (surface to ~10 cm) in order to better resolve the relationships between absorbance and fluorescence losses with depth. Fluorescence loss rates in experiments 4 and 8 were confirmed by examining the fluorescence loss rates in experiments 2, 3 and 7. The daily percentage changes of absorbance indices with depth were calculated for the data from experiments 4 and 8 (goal 2). Experiments 5–9 (in quartz tubes) examined the response of photo-oxidation rates to changes in light intensity (goal 3). In this analysis, the rate of photo-oxidation just below the surface (1.1 cm) was related to the mean daily ultraviolet radiation (UV-R) exposure. In late September-early October, the sun is near its seasonal equinox, and cloudy conditions were rare. Near the equator, the sun is directly overhead at the equinoxes. Experiments 7 and 8 examined how the rate of photo-oxidation changed with depth and estimated areal rates of photo-oxidation (goal 4).

### 2.4. Measurements

During each experiment, measurements of temperature and surface UV-AB radiation (UV-R) were collected every 30 min during sunlight hours, using a UV513AB Digital Light Meter (General Tools and Instruments, New York, NY, USA). The photocell collects both UV-A and UV-B radiation (280 nm–400 nm), although it is more sensitive to UV-A radiation (Suppl. Fig. S1). The General Tools light meter readings were compared with those of a Radiometer system (UVX Radiometer ART 97-0015-02, Radiometer Canada, London, ON, Canada) with UV-A and UV-B sensors to confirm sensitivity and allow comparison to other work (Suppl. Fig. S2A and B). The UV513AB Digital Light Meter was also calibrated against a Licor quantum sensor which collects all light, again to allow comparison to other work (Suppl. Fig. S2C and D). Each experimental light reading consisted of five measurements read just above the pool at one-minute intervals and averaged. The daily light exposure and daily temperature (experienced during the light period) were calculated from the area under the curve of the point-in-time averages plotted against time of day. Unfiltered pool water was collected at the beginning of each experiment to measure its absorbance and hence transmission of light.

At the end of the experiment, samples were analyzed for inorganic carbon (IC) as soon as they were removed from the pool (2018 only) to measure the amount of $CO_2$ produced due to photo-oxidation. IC is the sum of dissolved $CO_2$, $H_2CO_3$, $HCO_3^-$, and $CO_3^{-2}$. It is a more sensitive measure than DOC, thus providing better estimates of photo-oxidation. After each IC measurement, a subsample of the remaining water was removed for later analysis of DOC concentration, and absorbance and fluorescence profiles. All subsamples were stored in the dark at ≤4 °C.

Dissolved organic carbon and IC were measured on high temperature Shimadzu TOC-$V_{CSH}$ Total Organic Carbon (TOC) Analyzers (Shimadzu, Kyoto, Japan). The TOC analyzers were calibrated each day using standards made up from DOC and IC stock standard solutions. The DOC stock standard was made from special grade potassium hydrogen phthalate (>99.8% pure, Nacalai Tesque Inc., Kyoto, Japan), as per manufacturer's instructions. Inorganic carbon stock standard was made up from special grade sodium hydrogen carbonate and sodium carbonate (>99.5% pure, Nacalai Tesque, Kyoto, Japan) as per manufacturer's instructions. The DOC samples were removed from the fridge, allowed to warm up to room temperature and analyzed in small batches. As noted above, IC samples were not cooled but analyzed immediately after collection.

Absorbance profiles were measured on a SpectraMax Plus 384 spectrophotometer (Molecular Devices, Sunnyvale, CA 94089, USA) in 2015, and on a Genesys 10S UV–Vis Spectrophotometer (Daly City, California, United States), in 2018. Reference profiles of ultrapure water were run each day and subtracted from the experimental absorbance profiles before further analyses of the data. Absorbance indices ($ABS_{250-550}$, $ABS_{340}$, $Ka_{310}$, $Ratio_{254/365}$, $ABS_{250-550}.DOC^{-1}$, $SAC_{340}$, $SAC_{Ka310}$) and the Fluorescence Index (FI) provide information on DOC structure, source, aromaticity, and potential photo-reactivity (Table 2).

Fluorescence was measured on a SpectraMax Plus 384 spectrophotometer with fluorescence capabilities, in 2015. Ultrapure water controls were run each day and subtracted from the emission data. September 2018 fluorescence profiles were collected using a Horiba Aqualog (Horiba Ltd., Kyoto, Japan). Parallel factor analyses (PARAFAC) were performed in PLS Toolbox (Eigenvector Research, Wenatchee, WA, USA) on a Matlab platform (The Mathworks, Inc., Natick, MA, USA)

**Table 1**
Experimental treatments and mean physical conditions within the nine experiments (Exp) conducted in 2015 and 2018. These experiments investigated the rate of photo-oxidation of dissolved organic carbon in Rio Negro water and its relationships with light and depth. Depths are reported as the mid-depth of the experimental bottles in the water column. UV-R includes both UVA and UVB radiation. Temperature and light (UV-R) exposure were measured over the daylight hours so the daily average is for 12 h of daylight. n/a = data not available. See Sections 2.3–4 for experimental details.

| Year/month | Exp | Mid-depth of exposure (cm) | UV-R exposure Total (mW cm$^{-2}$) | Duration of experiment Daylight (h) | # of days | Daily UV-R (mW cm$^{-2}$ d$^{-1}$) | Temperature Mean Daily (°C) | Oxygen Initial (mg $O_2$ l$^{-1}$) |
|---|---|---|---|---|---|---|---|---|
| 2015 (Nov.–Dec.) | 1 | 2.75, 10.0, 22.5, 47.5 | 107.1 | 21.3 | 2 | 53.6 | 31.8 | 9.32 |
| | 2 | 2.75, 7.5, 22.5,47.5 | 170.5 | 32.1 | 2 | 56.6 | 32.2 | 7.98 |
| | 3 | 2.75, 7.5 | 122.7 | 34.2 | 3 | 30.8 | 29.7 | 8.35 |
| | 4 | 2.75, 4.5, 6.0, 7.5 | 131.2 | 25.1 | 4 | 43.4 | 30.9 | 7.75 |
| 2018 (Sept.–Oct.) | 5 | 1.1 | 101.7 | 18.0 | 3 | 50.8 | 31.4 | 6.96 |
| | 6 | 1.1 | 131.1 | 19.0 | 2 | 65.6 | 31.2 | 8.04 |
| | 7 | 1.1, 4.6, 7.1 | 117.3 | 18.8 | 2 | 58.7 | 31.5 | 9.15 |
| | 8 | 1.1, 2.1, 5.1, 8.1 | 123.4 | 18.9 | 2 | 61.7 | 32.2 | n/a |
| | 9 | 1.1 | 128.2 | 18.8 | 2 | 64.1 | 32.8 | 7.06 |

**Table 2**
Absorbance and fluorescence indices, their calculation, relevance and source. Paraphrased from Johannsson et al. (2017)

| | Name | Calculation | Relevance | References |
|---|---|---|---|---|
| Absorbance Indices | $ABS_{250-550}$ | Sum of absorbance of DOC from 250 to 550 nm | Measure of total absorbance | Johannsson et al., 2017 |
| | $ABS_{250-550}$ $DOC^{-1}$ | Sum of absorbance $DOC^{-1}$ | Measure of concentration-specific total chromophore absorbance | Ibid |
| | $ABS_{340}$ | Absorbance at 340 nm | Measure of aromaticity and protective potential of the DOC against some metals and ionoregulatory disturbance at low pH | Wood et al., 2011; Al-Reasi et al., 2011 |
| | $SAC_{340}$ | The specific absorbance at 340 nm (2.303 * absorbance at 340 nm $DOC^{-1}$ * 1000) | Same function, but now a concentration-specific characteristic of the DOC | Ibid |
| | $R_{254/365}$ | Ratio of absorbance at 254 nm to 365 nm | Index of the average molecular mass within the DOC | Dahlén et al., 1996 |
| | $Ka_{310}$ | Absorbance at 310 nm * (2.303 * $absorption_{310}$/pathlength (m)) | Related to the rate of oxygen radical (ROS) production during DOC photo-oxidation | Scully et al., 1996 Molot et al., 2005 |
| | $SAC_{Ka310}$ | $Ka_{310}$ index per unit of DOC | Measure of potential production of oxygen radicals concentration-specific to DOC | Ibid |
| Fluorescence Index | FI | Ratio of the emission at 450 nm to 500 nm, 370 nm excitation | Relative measure of the autochthonous vs allochthonous DOC source | McKnight et al., 2001 |

(DePalma et al., 2011; Al-Reasi et al., 2012). The selection of three fluorophore groups best resolved the 2018 data.

### 2.5. Fluorescence metrics

Goal 5, the development of fluorescence metrics for the Rio Negro, did not require a specific experiment. Dissolved organic carbon from forested ecosystems is composed of high proportions of humic acid-like (HA) and fulvic acid-like (FA) compounds. They are often accompanied by lesser amounts of tryptophan-like (TRPY) and tyrosine-like (TYR) components. Each set of compounds will fluoresce in defined regions of a fluorescence excitation-emission matrix (FEEM) when excited by specific wavelengths of light. These regions are referred to as fluorophores.

We used a published parallel factor analysis of Rio Negro water to define our fluorescence metrics (Johannsson et al., 2017). The water had been collected from the Anavilhanas Archipelago 110 km upstream of Manaus in December 2014. In 2015, the TYR response was not measured because it was outside the range of the fluorometer used in the present study. We picked four excitation wavelengths (250, 300, 325, and 370 nm) that, in combination, would pass through regions of strong emissions of each fluorophore. From Fig. 2, we determined which emission wavelengths corresponded to each fluorophore along each of the four excitation wavelengths (Table 3). The metrics were calculated by summing the fluorescence emissions across these set ranges of emission

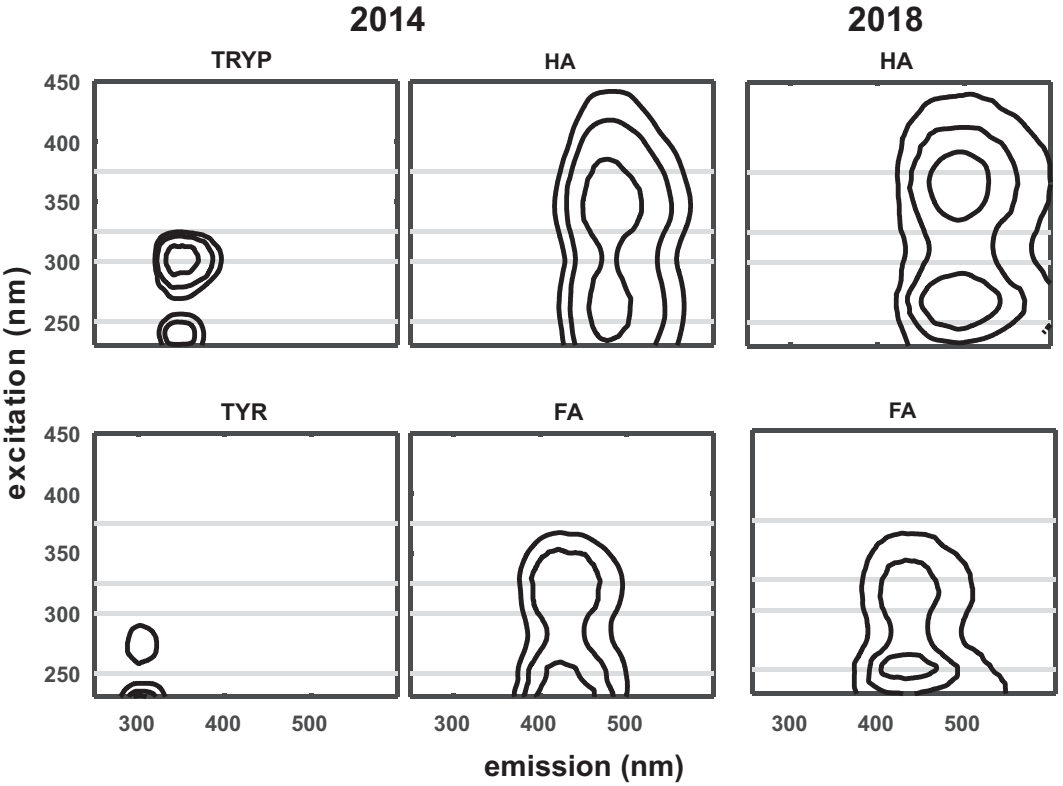


**Fig. 2.** Comparison of parallel factor analyses of Rio Negro water from 2014 and 2018. The 2014 water was collected offshore in the main channel of the Anavilhanas Archipelago in December (Johannsson et al., 2017, by permission of Elsevier). The 2018 water was collected offshore of Praia do Açutuba (Fig. 1) in September. HA represents the emission spectrum of humic acid-like substances, FA, fulvic acid-like substances, TRYP, tryptophan-like substances and TYR, tyrosine-like substances. Note that only the HA and FA panels are shown in 2018 as no TRYP or TYR signal was detected. The grey lines represent the four excitation wavelengths along which emission profiles were summed to calculate the fluorescence metrics (cf. Table 3).

wavelengths for each of the four excitation wavelengths separately. Excitation at 250 nm captured strong HA and FA fluorescence; 300 nm captured strong TRYP and FA fluorescence and to a lesser extent HA fluorescence; 325 nm captured FA and some HA fluorescence; and 370 nm, only captured HA fluorescence. Fluorescence at 370 nm was also required to calculate the fluorescence index (FI). FI is the ratio of the emission at 450 nm to the emission at 500 nm when excited at 370 nm (McKnight et al., 2001).

In order to determine if Rio Negro fluorescent regions and components were stable, we compared the 2014 and 2018 PARAFAC analyses. The 2018 water had been collected mid-channel off of Praia do Açutuba (offshore location in Fig. 1). If the fluorescent regions were stable, emission strengths of samples analyzed on the same instrument, could be quantified and compared over space and time.

### 2.6. Calculations

All data were converted to daily estimates in order to assemble consistent data across experiments.

#### 2.6.1. Daily rates of change of indices

*2.6.1.1. Time.* Experiments were run over two to four-day intervals. The absolute decrease in absorbance and fluorescence measures (and in total DOC) should be related to the concentration of DOC in the experimental water. The concentration of DOC will decrease during the first day of exposure, meaning that on the second day a smaller absolute amount of DOC (absorbance and fluorescence measures) will be lost. These proportionate decreases from day to day can be described by ln-linear relationships between the measure and time (days). We applied these relationships to calculate the change in each measure at the end of the first day of light exposure. IC increases but is dependent on the loss in DOC. Calculations determined that the correction for the exponential change in DOC was less than the SEM of the IC estimates. Therefore the estimates were divided by two, the number of days in these experiments.

Using the absorbance measure $Ka_{310}$, as an example:

The rate of change ($\%\,d^{-1}$) is given by the slope of the ln-linear relationship. This was calculated for both the dark controls and light treatments.

$$\text{Slope}_{(Ka310\ dark)} = \{[\ \ln(Ka_{310\ initial}) - \ln(Ka_{310\ dark\ (d=t)})]/t\} \quad (1)$$

$$\text{Slope}_{(Ka310\ light)} = \{[\ \ln(Ka_{310\ initial}) - \ln(Ka_{310\ light\ (d=t)})]/t\} \quad (2)$$

where, 't' is duration of the experiment in days, 'd' is day. 'Light' refers to the light-exposed treatment, 'dark' refers to the dark control treatment, and 'initial' refers to the $Ka_{310}$ value at the start of the experiment, which applies to both 'light' and 'dark' incubations. Change due to photo-oxidation is the difference between the 'dark' and 'light' treatments.

At $d = 1$:

$$Ka_{310\ dark\ (d=1)} = \exp[\ \ln(Ka_{310\ initial}) - \text{Slope}(Ka_{310\ dark})] \quad (3)$$

$$Ka_{310\ light\ (d=1)} = \exp[\ \ln(Ka_{310\ initial}) - \text{Slope}(Ka310_{light})] \quad (4)$$

The change in absorbance of $Ka_{310}$ due to photo-oxidation at the end of the first day of the experiment is:

$$\Delta Ka_{310\ (d=1)} = Ka_{310\ dark\ (d=1)} - Ka_{310\ light\ (d=1)}, \quad (5)$$

Changes during the first day of photo-oxidation will be referred to as $\Delta Index_{(d=1)}$ when more than one measure is considered.

*2.6.1.2. Depth.* Individual light wavelengths decay down a column of water exponentially and can be represented linearly by a ln-linear relationship with depth on the x-axis (Wetzel, 1975). The x-intercept of the relationship between $\ln(\Delta Index_{(d=1)})$ and depth would indicate the depth at which photo-oxidation of dissolved organic carbon could no longer be detected in this index. These depths were determined for absorbance and fluorescence indices for experiments 4 (2015) and 8 (2018) which each had four depth treatments within the depth range of photo-oxidative changes in absorbance.

#### 2.6.2. Light transmission through water

The absorbance profile of the pool water sets the distances that light wavelengths penetrate the water.

$$\text{Absorbance at wavelength } (\lambda), Abs(\lambda) = 0.4343\ \mu_{(\lambda)}\ d \quad (6)$$

where, 'd' is the depth of light passage in cm, and $\mu_{(\lambda)}$ is the linear attenuation coefficient for a given value of $\lambda$ in units of $cm^{-1}$ (www.physics.uoguelph.ca/~pgarrett/Teaching.html, 2016).

$$\mu_{(\lambda)} = Abs(\lambda)/0.4343 \text{ at } d = 1 \text{ cm} \quad (7)$$

Light decreases exponentially through the water column and the attenuation coefficient is the slope of that relationship. The depth of 1% light penetration of a specific wavelength is:

$$\text{Depth of light penetration } (\lambda)\ (1\%) = (\ \ln(100) - \ln(1))/\mu_{(\lambda)} \quad (8)$$

#### 2.6.3. Areal and surface IC production

In order to estimate IC production per day, daily light profiles were corrected to include the 6:00 a.m.–8:30 a.m. period when the pool was still covered by the tent. A graph of maximum UV-R values throughout the study was plotted against time of day (Suppl. Fig. S3). The light pattern over the day has a normal distribution, thus the values from 3:30 p.m. until 6:00 p.m. can represent the missing early morning hours as both periods were in light shade. The recorded UV-R exposure was augmented to include the early morning light. The amount of light received during the early morning hours was multiplied by the amount of IC production per unit of UV-R observed during the experiment. This value was added to the observed mg C $l^{-1}$ produced during the experiment. All 2018 experiments, except experiment 7, ran for exactly 48 h. Similar techniques were used to convert the data from experiment 7 to a 48 h-basis.

Areal production (mg C $m^{-2}\,d^{-1}$), the total amount of $CO_2$ produced by photo-oxidation under a square meter of river surface area, was

**Table 3**
Fluorescence metrics. Excitation wavelengths and their corresponding portions of the emission profile used to capture the fluorescence response of humic acid-like (HA), fulvic acid-like (FA) and tryptophan-like (TRYP) compounds. Results are based on PARAFAC analyses of Rio Negro water from the Anavilhanas Archipelago (Dec. 2014 Johannsson et al., 2017), and offshore of Praia do Açutuba (September 2018) (c.f. Fig. 1). The 2014 based metrics were used throughout the present study.

| Excitation | December 2014 | | September 2018 | |
|---|---|---|---|---|
| Wavelength (nm) | Emission response range (nm) | Composition | Emission RESPONSE RANGE (nm) | Composition |
| 370 | 400–550 | HA | 400–600 | HA |
| 325 | 400–450 | FA | 370–450 | FA |
| | 460–550 | HA | 460–600 | HA |
| | 330–370 | TRYP | | |
| 300 | 400–450 | FA | 370–460 | FA |
| | 460–550 | HA | 470–600 | HA |
| 250 | 400–450 | FA | | |
| | 460–550 | HA | | |

**Table 5**
Comparison of literature rates of photo-oxidation of dissolved organic carbon from the Rio Negro. When rates were measured over the mid-day period only, they were corrected to whole day estimates by dividing by 0.75 (Granéli et al., 1998). Hourly rates were converted to daily rates of 12 h.

| Authors | Location | Method | Original rate | Daily rate (mg C $l^{-1}$ $d^{-1}$) |
|---|---|---|---|---|
| Amon and Benner (1996a) | Rio Negro 3 km upstream of Manaus | River water flow-through system, not filtered, mid-bottle depth approx. 4 cm, pyrex bottles, 28 °C, whole day, Mar.-April 1993 | 4.5 μM C $h^{-1}$ | 0.65[a] |
| Granéli et al. (1998) | Rio Negro up stream of Manaus, DOC = 9.9 mgl.$^{-1}$ | Pool on shore, 0.2-μm filter, quartz tubes half out of water lengthwise, 6 h, 35 °C, mid-day period Jan 1996 | 0.7 mg $l^{-1}$ 6 $h^{-1}$ | 0.93 |
| Johannsson et al. (2017) | Rio Negro 110 km upstream of Manaus, lake in archipelago, DOC = 9.1 mg $l^{-1}$ | River flow through system in white trays, 0.45-μm filter, flint quartz bottles just below surface, 15.5 h, 30–32 °C, Dec. 11, 2014 | 0.46 mg C $l^{-1}$ $d^{-1}$ | 0.46 |
| Johannsson et al. (2017) | Rio Negro 110 km upstream of Manaus, main channel, DOC = 10.6 mg $l^{-1}$, | Ibid, 10.3 h, 30–34 °C, Dec. 122,014 | 1.17 mg C $l^{-1}$ $d^{-1}$ | 1.17 |
| Present study | Rio Negro – upstream of Manaus, main channel, DOC = 10.8 mg $l^{-1}$ | Pool containing Rio Negro water, 0.45-μm filter, quartz tubes, 1.1 cm mid-bottle depth, 48 h, $n$ = 5, 29–36 °C, Sept. 22–Oct. 18, 2018 | 0.41–0.68 mg C $l^{-1}$ $d^{-1}$ | 0.41–0.68 |

[a] Not corrected for 50% loss of UVA and 20% loss of UVB in pyrex bottles.

calculated from the graph of the rate of production of IC versus depth in the water column. Exponential decay curves were fitted to the data: $Y = a(1- K)^{dp}$ where 'a' is the y intercept (mg C.$l^{-1}$.$d^{-1}$), 'dp' is the depth (cm) and K is the rate of change per cm of depth: The curves were terminated at a depth of 20 cm based on the data from experiments 7 and 8. The area under this curve is the total $CO_2$ production due to photo-oxidation in units of mg C $l^{-1}$ $d^{-1}$ over 20 cm depth. These data were converted to mg C $m^{-2}$ $d^{-1}$.

### 2.7. Statistics

For all measures (IC, DOC, fluorescence and absorbance), the light-exposed data were subtracted from the mean of the dark control data (or the combination of dark and initial data if these were not significantly different) in order to calculate the change due to light exposure. Thus, positive changes are a loss or decrease and negative changes are a gain or increase. The data for each treatment were checked for normality of distribution using the Shapiro-Wilk Normality Test, which determined whether parametric or non-parametric tests would be applied. Parametric tests included ANOVA followed by Tukey's multiple comparison test, or Student's *t*-tests. Non-parametric tests included Kruskal-Wallis one-way ANOVA on ranks followed by Dunn's multiple comparisons test or the Mann-Whitney *U* test for a two treatment comparisons. Curves were fitted to data using linear regression or exponential relationships. All analyses were carried out in Graphpad PRISM 7 (Graphpad Software Inc., CA, USA). The significance level was set at 0.05 and data are reported as means ±1 SEM (n), unless otherwise noted.

## 3. Results

### 3.1. DOC

The concentration and characteristics of DOC in collected Rio Negro water differed between November 2015 and October 2018 (Suppl. Table S1). The concentration of DOC was lower in November 2015 than in September 2018: 8.7 ± 0.1 (24) mg C $l^{-1}$ compared with 10.8 ± 0.1 (48) mg C $l^{-1}$.

### 3.2. Depth of photo-oxidation (goal 1)

Not all photo-oxidation is complete, ending in the production of $CO_2$ and CO. Section 3.5 examines the depth pattern of complete photo-oxidation. Partial photo-oxidation results from changes in DOC when it does not degrade sufficiently to produce $CO_2$ and CO. Sections 3.2.1 and 3.2.3 look at the depth of photo-oxidation effects as seen through changes in absorbance and fluorescence. These changes were due to both complete and partial photo-oxidation.

#### 3.2.1. Absorbance

In both 2018 and 2015, daily rates of change ($\Delta Index_{(d=1)}$) of absorbance indices decreased significantly with depth. Note that the positive values of $ABS_{250–550}$, $ABS_{340}$ and $Ka_{310}$ indicate losses (Figs. 3 and 4A, B and C), while the negative values of $R_{254/365}$ indicate increases (Figs. 3 and 4D). The exponential decay relationship best captured the changes in the indices in 2018 especially as some of the indices did not decrease to zero. As mentioned in 2.6.3, Y approaches but does not reach the X-

**Table 4**
The effect of loss of UVB and shorter UVA wavelengths (280 nm–345 nm) on photo-oxidation. Specific rates of daily change (% $d^{-1}$) of DOC (experiments 5–9) and absorbance indices (experiment 8) due to photo-oxidation over depth. Mid-tube depths were 1.1 cm, 2.1 cm, 5.1 cm and 8.1 cm. Estimates for 2.75 cm depth, the mid-depth of flint-quartz bottles (experiments 1–4), were either interpolated from the 2.1 cm and 5.1 cm data, or they were predicted from Eqs. (9) to (12) (Section 3.3), assuming 61.3 mW $cm^{-2}$ UV-R, the daily UV-R of experiment 8. PR = percentage of the flint-quartz response to the quartz response.

| Index | Experiment | UV-R | | | (% change $d^{-1}$) | | | | |
|---|---|---|---|---|---|---|---|---|---|
| | | | | | Interpolated | Predicted | PR | | |
| | | (mW $cm^{-2}$) | 1.1 cm | 2.1 cm | 2.75 cm | 2.75 cm | (%) | 5.1 cm | 8.1 cm |
| DOC | 6–9 | 58.7–65.6 | 2.1–5.7[a] | 3.0 | 1.8 | | | 1.6 | 0.0 |
| $ABS_{250\_550}$ | 8 | 61.3 | 12.0 | 9.6 | 8.4 | 3.1 | 36% | 5.3 | 2.2 |
| $ABS.DOC^{-1}$ | 8 | 61.3 | 9.3 | 6.9 | 5.7 | | | 3.8 | 2.2 |
| $ABS_{340}$ | 8 | 61.3 | 13.7 | 11.1 | 10.0 | 3.9 | 39% | 6.2 | 3.5 |
| $SAC_{340}$ | 8 | 61.3 | 11.1 | 8.4 | 7.3 | | | 4.7 | 3.5 |
| $Ka_{310}$ | 8 | 61.3 | 13.9 | 11.1 | 9.9 | 3.7 | 37% | 5.9 | 3.1 |
| $SAC_{Ka310}$ | 8 | 61.3 | 11.3 | 8.4 | 7.2 | | | 4.4 | 3.1 |
| $R_{254/365}$ | 8 | 61.3 | 4.4 | 3.8 | 3.3 | 2.1 | 60% | 2.1 | 2.0 |

[a] DOC change in experiment 8 at 1.1 cm depth was low (2.1%) and did not follow the changes in IC. The specific rate of change of DOC in the other three experiments ranged from 3.0 to 5.7% at 1.1 cm depth. DOC data from experiment 5 were unavailable.

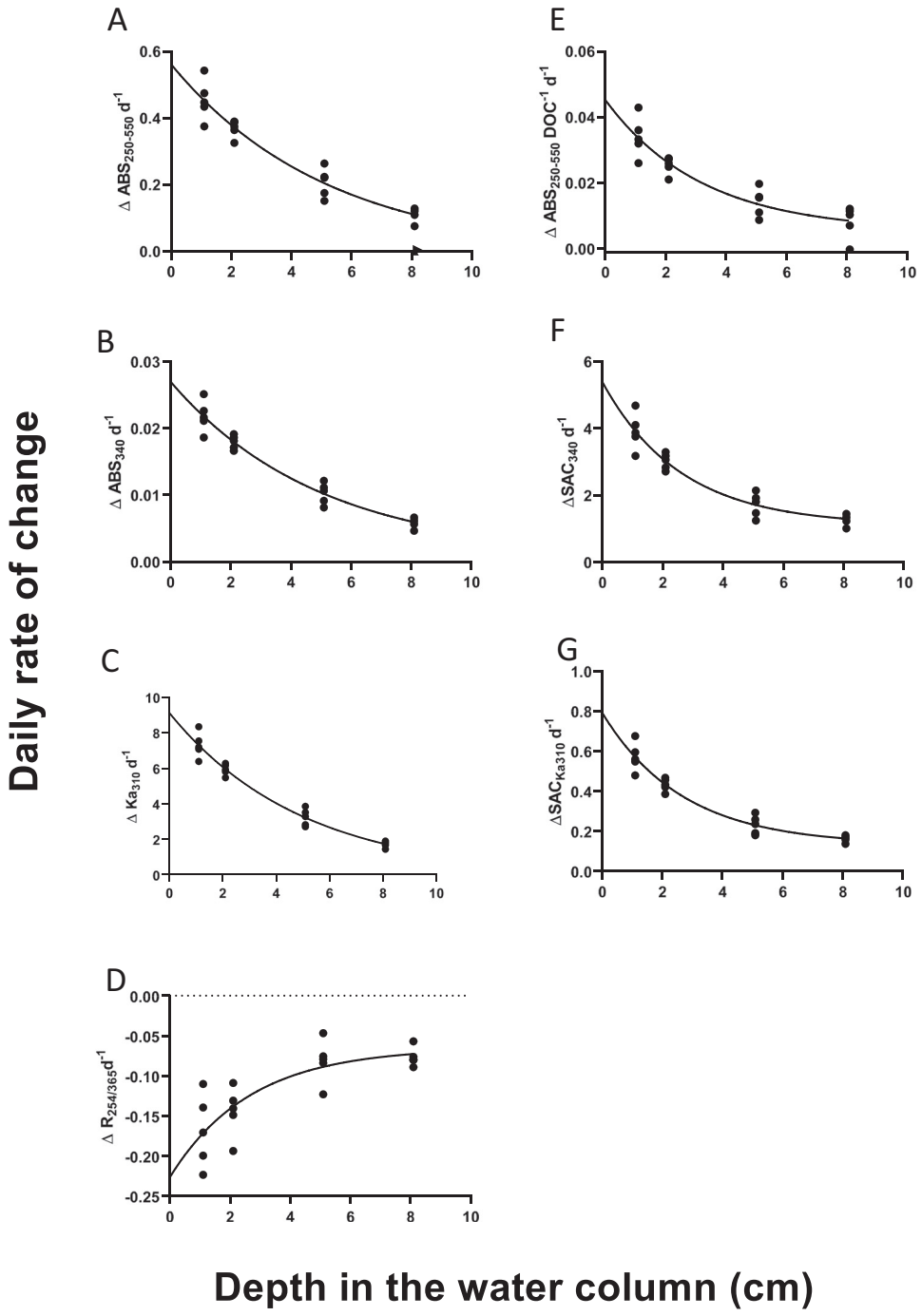


**Fig. 3.** 2018 – Decay of absorbance indices with depth - experiment 8 (quartz tubes). Exponential decay models were fitted to the data. $n = 20$ with the exception of (A) where $n = 19$. An equation could not be fitted to (A) when the excluded value (▲) was present in the analysis. 'db' is the depth in cm. Depths at which the response had declined by 95% are given in square brackets. If the relationship plateaued significantly above zero (i.e. >2SEM above zero) indicating that the DOC had become recalcitrant, then the plateau is give in {} brackets. (A) $\Delta ABS_{(250-550)}$ $d^{-1} = 0.6213$ (1–0.2082)$^{db}$, SS = 0.0351, Sy.x = 0.0468, $R^2 = 0.9208$, [14 cm]. (B) $\Delta ABS_{340}$ $d^{-1} = 0.0302$ (1–0.2194)$^{dp}$, SS ≤0.0001, Sy.x = 0.0018, $R^2 = 0.9491$, [14 cm]. (C) $\Delta Ka_{310}$ $d^{-1} = 10.17$ (1–0.2201)$^{dp}$, SS = 4.642, Sy.x = 0.5225, $R^2 = 0.9628$, [14 cm]. (D) $\Delta R_{254/365}$ $d^{-1} = -0.2181$ (1–0.3736)$^{dp}$, SS = 0.0148, Sy.x = 0.0295, $R^2 = 0.6577$, [8 cm,] {−0.0637}. (E) $\Delta ABS_{(250-550)}$ $DOC^{-1}d^{-1} = 0.0495$ (1–0.3303)$^{dp}$, SS = 0.0004, Sy.x = 0.0050, $R^2 = 0.8452$ [9 cm]. (F) $\Delta SAC_{340}$ $d^{-1} = 5.962$ (1–0.4002)$^{dp}$, SS = 2.637, Sy.x = 0.3939, $R^2 = 0.9101$ [8 cm] {1.165}. (G) $\Delta SAC_{Ka310}$ $d^{-1} = 0.8741$ (1–0.3908)$^{dp}$, SS = 0.0438, Sy.x = 0.0438, $R^2 = 0.9354$ [8 cm] {0.1386}.

axis (or plateau). The water depths at which change in the absorbance index had decreased by 95% were 14 cm for $ABS_{340}$, $Ka_{310}$, and $ABS_{250-550}$ and 8.0 cm for the $R_{254/365}$. These are within 1SEM of the estimate of the asymptote; thus not significantly different from zero change. The daily rates of change of two absorbance indices standardized to DOC concentration ($SAC_{340}$, and $SAC_{Ka310}$) reached a plateaued significantly above Y = 0 (Figs. 3F and G), indicating that some of the DOC was recalcitrant.

In 2015, the exponential relationship was statistically 'ambiguous', and the data were fitted well by linear and ln-linear relationships (Figs. 4A to D) with $R^2$ values of 0.5148 to 0.7705. We suspect the ambiguity of the exponential decay fit may be related to large variability in the data. One was added to the daily changes in most indices because some of the daily changes were negative at depth and it is not possible to calculate the natural logarithm of a negative number. The x-intercepts ranged from 10 to 12 cm. The slopes of these relationships

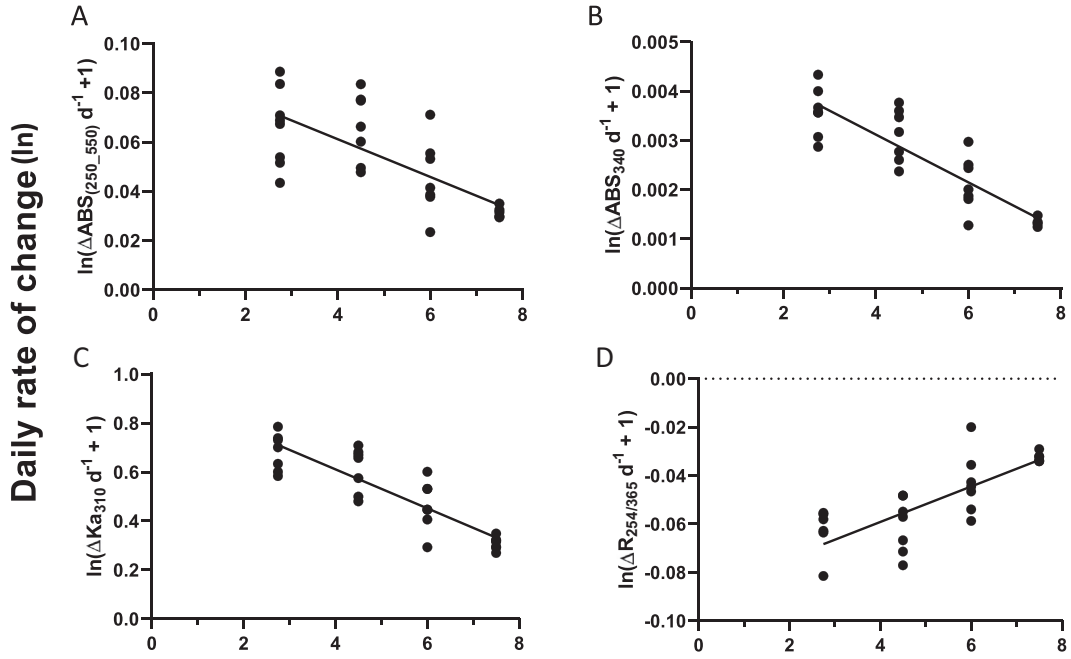


**Fig. 4.** 2015 – Decay of abundance indices with depth – experiment 4 (flint bottles). Relationships between the ln(daily rates of change of absorbance indices) [ln ($\Delta Index_{(d=1)} + 1$)] and water column depth (cm). All F values were > 27 *p* values were < 0.0004 and df values were (1,25). X-intercepts appear in square brackets. (A) $\ln(\Delta ABS_{(250-550)}\, d^{-1} + 1) = -0.007571 * Depth + 0.09168$, $R^2 = 0.5148$ [12 cm]. (B) $\ln(\Delta ABS_{340}\, d^{-1} + 1) = -0.0004841 * Depth + 0.005056$, $R^2 = 0.7705$ [10 cm]. (C) $\ln(\Delta\, Ka_{310}\, d^{-1} + 1) = -0.0710 * Depth + 0.9182$, $R^2 = 0.7619$ [13 cm]. (D) $\ln(\Delta R_{254/365}\, d^{-1} + 1) = 0.007393 * Depth - 0.08855$, $R^2 = 0.6155$ [12 cm].

are the rates of change in $\Delta Index_{(d=1)}$ with depth. As DOC did not change detectibly in 2015, these relationships also represented the changes in $SAC_{340}$, $ABS_{250-550}.DOC^{-1}$, and $SAC_{Ka310}$ with depth.

*3.2.2. Environmental influences on absorbance losses*

Although UV-R, temperature and unfiltered pool water transparency were measured for each experiment in 2015, the three variables were

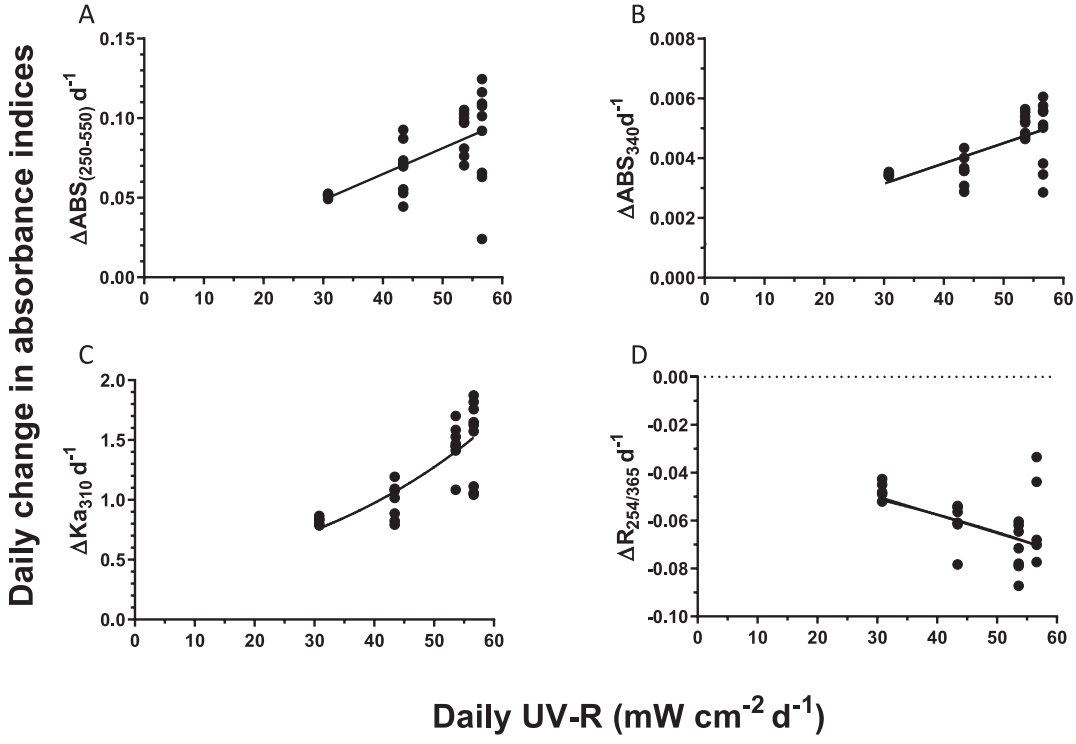


**Fig. 5.** Effect of UV-R exposure on daily changes in absorbance indices ($\Delta Index_{(d=1)}$): experiment 4 (flint bottles at 2.75 cm depth). (A) $\Delta ABS_{(250-550)}\, d^{-1} = 0.001624 * UV\text{-}R\ (mW\ cm^{-2}) - 9.859e{-}005$: $F_{(1,18)} = 16.02$, $p = 0.0004$, $R^2 = 0.3639$: (B) $\Delta ABS_{340}\, d^{-1} = 6.771e{-}005 * UV\text{-}R\ (mW\ cm^{-2}) + 0.001118$: $F_{(1,27)} = 19.36$, $p = 0.0002$, $R^2 = 0.41.76$: (C) $\Delta Ka_{310}\, d^{-1} = 0.3328 * \exp(0.0268 * UV\text{-}R)$: SS = 1.364, Sx.y = 0.2248, $R^2 = 0.6194$, $n = 29$. (D) $\Delta R_{254/365}\, d^{-1} = -0.0007638 * UV\text{-}R\ (mW\ cm^{-2}) - 0.027$: $F_{(1,26)} = 9.641$, $p = 0.0046$, $R^2 = 0.2705$.

highly correlated. The effect of temperature on changes in DOC absorbance was measured in the dark-control treatments: little or no changes were observed in these samples indicating that temperature variation amongst the experiments was not important. Pool water transparency was likely a minor factor affecting surface water samples because only 0.5 cm of pool water covered the experimental bottles, which were 5 cm in diameter. This leaves light (UV-R) as the only likely variable driving changes in absorbance in our experiments. The daily change in absorbance indices in the near-surface (2.75 cm) samples increased significantly with greater UV-R exposure, with $R^2$ values of 0.2705 to 0.6194 (Fig. 5A–D).

*3.2.3. Fluorescence*

In 2018 (experiment 8), fluorescence changes were best captured by ln-linear relationships not exponential relationships. This is likely due to the variability in the FI data, and to the short depth range studied, compared with the total depth range of HA losses in fluorescence. Photooxidation caused a decrease in FI: the decreases became smaller with depth and ceased by 10 cm. (the x-intercept in Fig. 6A). Humic acid-like fluorescence losses, at 370 nm excitation, declined with depth (Fig. 6B): the ln-linear relationship indicated that changes in fluorescence extended down to 43 cm depth (Fig. 6B). The specific rate of loss in the top 7.5 cm ranged from 6% $d^{-1}$ at 1.1 cm depth to 3% $d^{-1}$ at 8.1 cm depth. No significant changes in HA with depth were observed at 300 or 325 nm: in fact, most changes observed were not significantly different from zero. Fulvic acid-like fluorescence increased when exposed to light at both 300 nm (ΔFA = 20 FU.$d^{-1}$, specific rate of change = 48% $d^{-1}$) and at 325 nm (ΔFA = 33 FU $d^{-1}$, specific rate of change = 9% $d^{-1}$) with no apparent relationship to depth (data not shown).

In 2015, HA fluorescence declined significantly with depth at all four excitation wavelengths (Fig. 7A, 8A–D). The ln-linear relationships of HA fluorescence loss, ceased at 35, 34, 25 and 25 cm, respectively, where the relationships encountered the x-axis (Fig. 7A). FA and TRYP generally lost fluorescence at 2.75 and 4.5 cm depth, the exception being FA at 250 nm, 4.5 cm depth, which showed no significant change (Fig. 8B, C, D and E). At deeper depths no gains or losses were detected in FA or TRYP. FI decreased in the upper portions of the water column (2.75 and 4.5 cm) and increased at depth (7.5 cm in experiment 4) (Fig. 8F). The patterns of loss in HA fluorescence in experiments 2, 3 and 7 were similar to or greater than those in experiments 4 and 8. HA x-intercepts were > 24 cm depth, with one exception (out of 14 HA depth series). In 2015, all FA x-intercepts were < 12 cm (data not shown). No fluorescence data were collected in experiment 1.

*3.2.4. Pool light (UV-R) versus HA fluorescence losses*

Transmission of light through water is dependent on the length of the wavelength of light, the longer wavelengths penetrating more deeply. A plot of 1% UV-R penetration depths for experiment 4 pool water (Fig. 7B), indicated that only the longest UV wavelengths could reach 35 cm depth in the pool during experiment 4. At 35 cm depth, the x-intercept at 370 nm excitation, wavelengths with 1% penetration fell between 390 and 400 nm (highest UVA radiation). At 25 cm depth, the wavelengths of 1% penetration fall between 380 and 390 nm (long UVA radiation). At 10 to 12 cm depth, where absorbance indices cease changing, wavelengths of 320–340 nm have declined to 1% penetration.

*3.3. Specific rates of change (goal 2)*

In the near-surface samples at 1.1 cm depth, specific rates of change of the absorbance indices ranged from 9.3 to 13.9% $d^{-1}$ and were higher than those of DOC at ~5% $d^{-1}$ (Table 4). $R_{254/365}$ was the exception with a specific rate of change of 4.4% $d^{-1}$ (Table 4). At 7.5 cm depth, the specific rates of change fell to between 2.0 and 3.5% $d^{-1}$ with the exception of DOC which was below detection.

Specific rates of change in 2015 ranged from 1.9 to 3.8% $d^{-1}$ at 2.75 cm depth (experiments 1 to 4), to 0.9 to 1.7% $d^{-1}$ at 7.5 cm depth (experiments 3 and 4) (Suppl. Table S2). Specific rates of change at 2.75 cm depth varied significantly with the daily UV-R experienced (Eqs. (9)–(12)). These relationships were employed to compare losses in quartz tubes to those in flint bottles which have reduced transmission of UV-R.

$$\Delta ABS_{250\text{–}550}\left(\%d^{-1}\right) = 0.05025 * \text{daily UV}-\text{R} + 0.008799,\ F_{(1,28)} = 15.89, p = 0.0004, R^2 = 0.3620 \quad (9)$$

$$\Delta ABS_{340}\left(\%d^{-1}\right) = 0.05042 * \text{daily UV}-\text{R} + 0.8404,\ F_{(1,27)} = 20.03, p = 0.0004, R^2 = 0.429 \quad (10)$$

$$\Delta Ka_{310}\left(\%d^{-1}\right) = 0.06451 * \text{daily UV}-\text{R}-0.2587,\ F_{(1,27)} = 39.68, p<0.0001, R^2 = 0.5951 \quad (11)$$

$$\Delta R_{254/365}\left(\%d^{-1}\right) Y = -0.02047 * \text{daily UV}-\text{R}-0.7529,\ F_{(1,26)} = 9.417, p = 0.0050, R^2 = 0.2659 \quad (12)$$

Specific rates of change in 2015 were estimated at the 2018 daily UV-R of 61.3 mW $cm^{-2}$ using Eqs. (9) to (12) above. They were compared with 2018 specific rates of change calculated for 2.75 cm depth, as interpolated from the 2.1 cm and 5.1 cm data (Table 4). The mid-bottle depth of the flint bottles was 2.75 cm. The specific rates of change determined from the 2015 relationships were 37–39% of the values determined from the 2018 interpolation, with the exception of the specific rate of $R_{254/365}$ which was 60% of the 2018 value.

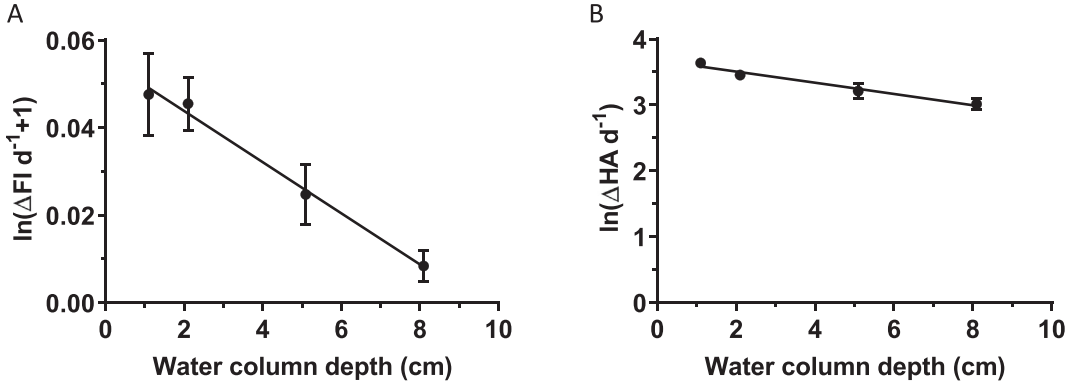


**Fig. 6.** 2018 Effect of depth on daily rates of change of (A) FI and (B) HA- experiment 8, (quartz tubes). (A) $\ln(\Delta FI\ d^{-1} + 1) = -0.005847 * \text{Depth (cm)} + 0.05557$, $F_{(1,2)} = 244.1$, $p = 0.0042$, $R^2 = 0.9919$, x-intercept = 10 cm. (B) $\ln(\Delta H \cdot d^{-1}) = -0.08507 * \text{Depth (cm)} + 3.679$, $F_{(1,2)} = 65.77$, $p = 0.0149$, $R^2 = 0.9705$, x-intercept = 43 cm.

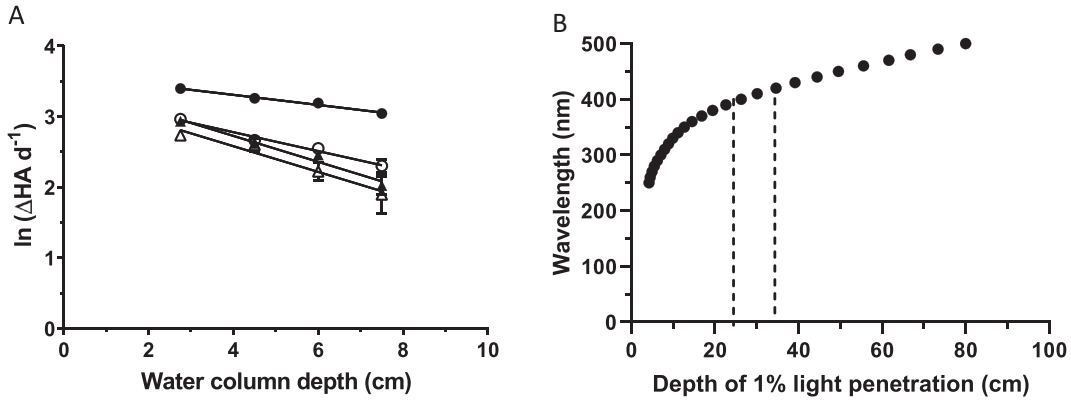


**Fig. 7.** (A). Effect of depth on daily rates of change of HA at four excitation wavelengths – 370 nm, 325 nm, 300 nm, and 250 nm - experiment 4 (flint bottles). The x-intercept is given in []. The linear regressions were: 370 nm, $\ln(\Delta HA\ d^{-1})$ (FU) = −0.1245 * Depth (cm) + 4.396: $F_{(1,2)} = 56.2$, $p = 0.0173$, $R^2 = 0.9656$, [35 cm]. 325 nm, $\ln(\Delta HA\ d^{-1})$ (FU) = −0.1072 * Depth (cm) + 3.613; $F_{(1,2)} = 121.8$, $p = 0.0081$, $R^2 = 0.9838$, [34 cm]. 300 nm, $\ln(\Delta HA\ d^{-1})$ (FU) = −0.1367 * Depth (cm) + 3.368; $F_{(1,2)} = 134.4$, $p = 0.0074$, $R^2 = 0.9853$, [25 cm]. 250 nm, $\ln(\Delta HA\ d^{-1})$ (FU) = −0.1272 * Depth (cm) + 3.235; $F_{(1,2)} = 40.8$, $p = 0.0236$, $R^2 = 0.9533$, [25 cm]. (B) The 1% penetration depth of ultraviolet and some PAR wavelengths in experiment 4 pool water. The dashed lines delimit the range of depths at which HA fluorescence changes ceased along the four excitation wavelengths in experiment 4 (panel (A) above): 25 cm and 35 cm. See Section 2.6.2 for description of calculations.

### 3.4. Rates of photo-oxidation

#### 3.4.1. Relationship of near-surface photo-oxidation and UV-R (goal 3)

Changes in DOC with photo-oxidation were too small to measure reliably in 2015, using measures of DOC concentration, therefore IC measurements were used in 2018.

The observed rates of daily photo-oxidation near the surface (1.1 cm) in 2018 ranged between 0.39 ± 0.07 ($n = 8$) and 0.68 ± 0.07 ($n = 4$) mg C $l^{-1}$ $d^{-1}$ over the five experiments 5–9 (Fig. 9). A strong relationship existed between daily IC production and daily UV-R in 2018 ($R^2 = 0.9162$) at the surface (1.1 cm). No photo-oxidation was detected at UV-R levels below 29.6 mW $cm^{-2}$ $d^{-1}$. Given this high x-intercept, we checked the low light sensitivity of the General Tools Digital Light Meter by comparing it against the more well-known Radiometer light meter with UVA and UVB sensors, and with the LiCor quantum sensor which records all light. The linear relationships extended to the lowest readings (Suppl. Fig. S2A, B, C and D).

#### 3.4.2. Areal rates of photo-oxidation (goal 1 and 4)

In the vertical profile, photo-oxidation of DOC to IC decreased down through the water column exponentially with an $R^2$ of 0.9665 (experiment 8): and 0.9761 (experiment 7) (Fig. 10).Extending these graphs

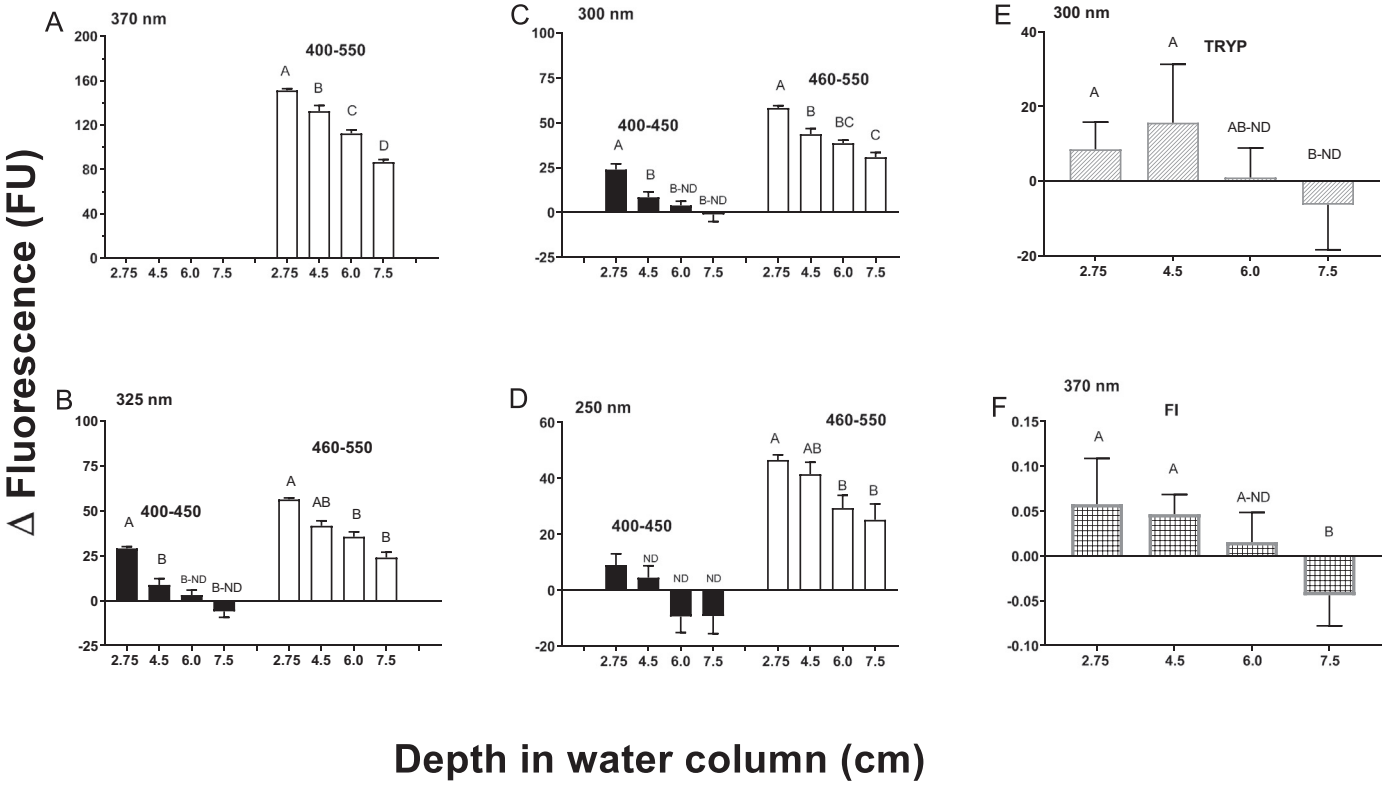


**Fig. 8.** 2015 Photo-oxidation induced changes in fluorescence with depth - experiment 4 (flint bottles). (A–D): responses of fulvic-like moieties (FA) (solid bars), and humic-like moieties (HA) (open bars) to excitation at (A) 370 nm (B) 325 nm, (C) 300 nm, and (D) 250 nm: emission ranges given above the bars. (E) response of tryptophan-like moieties (TRYP) (330 nm to 370 nm) at 300 nm excitation, and (F) the fluorescence Index (FI). Significant differences within a component between depths are indicated by different letters above the bars.

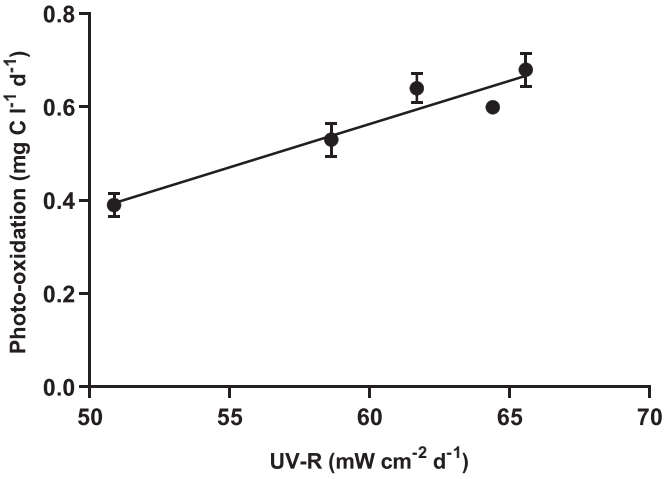


**Fig. 9.** Relationship between daily rate of photo-oxidation of DOC and daily UV-R at the water's surface (1.1 cm depth). Collation of data from experiments 5–9 (quartz tubes). Means ±1SEM ($n$ = 3 to 8). Experiments were conducted in quartz tubes. Rate of photo-oxidation (mg C $l^{-1}$ $d^{-1}$) = 0.01855 ∗ UV-R (mW $cm^{-2}$ $d^{-1}$) − 0.5491, $F_{(1,3)}$ = 32.80, $p$ = 0.0106, $R^2$ = 0.9162, x-axis intercept = 29.6 mW $cm^{-2}$.

to the y-axis predicted that the rates of photo-oxidation at the surface were 0.80 and 0.86 mg C $l^{-1}$ $d^{-1}$ in experiments 7 and 8 respectively. The curves tended to but never reached zero: they approached this plateau between 9 and 15 cm depth. The rate of photo-oxidation had decayed by 95% by this point. These depths are similar to or slightly shallower than those for the loss of absorbance (Section 3.2.1). The areal rates, calculated to a depth of 20 cm, were 28.8 and 39.3 mg C $m^{-2}$ $d^{-1}$ for experiments 7 and 8 respectively. These represent a loss of 1.33 to 1.82% of DOC C $d^{-1}$ in the top 20 cm at the DOC concentration of 10.8 mg C $l^{-1}$. It should be noted that the pool water was changed immediately before the start of experiment 7 and was darker in colour than on other occasions.

### 3.5. Fluorescence metrics (goal 5)

The individual excitation and emission wavelengths chosen to characterize the 2014 FA and HA signals, also captured the fluorophores well in 2018 (Fig. 2, Table 2). The 2014 PARAFAC analysis indicated an overlap of TRYP and FA emission signals between 370 nm and 400 nm (Fig. 2). We defined the end of the TRYP signal at 370 nm and the start of the FA signal as 400 nm. HA fluorescence at all excitation wavelengths, could be extended to 600 nm in new studies. Comparison of emission profiles before and after photo-oxidation (experiment 9) showed that 450 nm is the correct divide between FA and HA components (Suppl. Fig. S4B, and C). FA and HA emission signals overlap between 400 and 500 nm, After photo-oxidation, the emissions increased below 450 nm and decreased above 450 nm, at both 300 and 325 nm excitation, indicating that 450 nm was a natural divide (Suppl. Fig. S4B and C). Overall, the fluorophore regions were stable between 2014 and 2018.

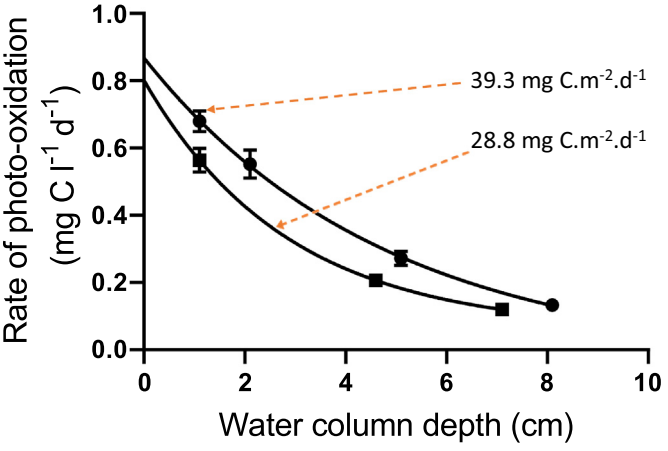


**Fig. 10.** Decay of photo-oxidation with depth. Exponential decay models were fitted to the data from experiment 7 (▪) and experiment 8 (●). Experiment 7, rate of photo-oxidation = $0.80(1–0.3507)^{dp}$, $R^2$ = 0.9761, df = 7; and experiment 8 rate of photo-oxidation = 0.86(1.0–0.2098)dp, R2 = 0.9665, df = 9. Dp = depth.

## 4. Discussion

From climate change, to deforestation, farming practices, fisheries exploitation, and mining, strong forces are altering the Amazon Basin. These forces can alter the processing of decaying plant material as well as the types of terrestrial and aquatic plant material available for decay. Our study was designed to provide present day, basic understanding of the process of photo-oxidation in the Rio Negro.

### 4.1. Rates of photo-oxidation

#### 4.1.1. Comparison of 'surface' rates

Three previous studies have measured rates of photo-oxidation in Rio Negro water under near-surface conditions (Amon and Benner, 1996a; Granéli et al., 1998; Johannsson et al., 2017) (Table 5). Estimates range from 0.41 to 1.17 mg C $l^{-1}$ $d^{-1}$: Much of this variation is probably due to differences in methodology and light intensity because DOC concentrations were likely similar - approximately 10 mg C $l^{-1}$. The work most comparable to the present study in technique and results was that of Granéli et al. (1998). They situated quartz tubes horizontally at the air/water interface in a pool with a flow-through system (water source not identified). Their surface rates of photo-oxidation were 0.93 mg C $l^{-1}$ $d^{-1}$ which is in line with the 'at surface' estimates of 0.80 and 0.86 mg C $l^{-1}$ $d^{-1}$ in the present study (Fig. 10).

Johannsson et al.'s (2017) study likely overestimated the rate of photo-oxidation at 1.17 mg C $l^{-1}$ $d^{-1}$ at 2.75 cm depth, because they exposed their bottles to sunlight in shallow white trays which would have reflected a significant amount of light back into the bottles. They also used flint-quartz bottles with reduced UV transmittance (Section 2.2).

The rates observed by Amon and Benner (1996a) (0.65 mg C $l^{-1}$ $d^{-1}$ at ~4 cm depth) were obtained by very different methods (Table 5). Their experimental design should have resulted in rates lower than in the present study due to the greater depth at which their experimental pyrex bottles were held and the reduced transmittance of UV-R by pyrex (Table 5). At the same time, the experimental water was not filtered, allowing particulate organic carbon (POC) to be photo-oxidized as well as the DOC. The data of Porcal et al. (2013b, 2015) support the possibility that some POC, normally removed by 0.45-μm filters, is photo-oxidizable. The relatively higher rate of photo-oxidation of Amon and Brenner (1996) and the work of Porcal et al. (2013b, 2015) suggest that estimates of $CO_2$ production from DOC alone may underestimate the actual daily rates of photo-oxidation of organic carbon in the river. Consequently, the rates of Granéli et al. (1998) and the present study may underestimate the return of $CO_2$ to the atmosphere via photo-oxidation because POC degradation was excluded.

The surface and subsurface (1.1 cm water depth) rates of photo-oxidation of DOC from the present study, during the season of high solar radiation are greater than or in line with literature estimates for other natural water bodies. The specific rate of loss of DOC in the present study were similar to those of Molot et al. (2005) and Porcal et al. (2013a) for boreal streams (4 to 8% $d^{-1}$ under peak conditions or 3 to 5% $d^{-1}$ under maximum light conditions) vs 2.1 to 5.7% $d^{-1}$ for the Rio Negro under maximum light conditions (Table 4). Surface rates in the present study (0.80 and 0.86 mg C $l^{-1}$ $d^{-1}$) were higher than summer surface rates of IC production for high latitude lakes in Sweden and Finland of similar DOC content (Granéli et al., 1996 from Fig. 2,

recalculated as 0.31 and 0.41 mg C $l^{-1}$ $d^{-1}$, DOCs = 9.7 and 11.2 mg $l^{-1}$; Vähätalo et al., 2000, from Fig. 3, maximum of 0.40 mg C $l^{-1}$ $d^{-1}$ in Lake Valkea-Kotinen, DOC = 12.1 $l^{-1}$). Rates of photo-oxidation of DOC in the Rio Negro were higher than those measured by Suhett et al. (2007) in a tropical lagoon on five of their six sampling occasions when adjusted for a DOC of 10 mg $l^{-1}$ (Figs. 2A, B in Suhett et al., 2007,). These comparisons, particularly of rivers versus lakes/lagoons support the hypotheses that photo-oxidation rates in rivers are greater than those in lakes, that total photo-oxidation at the surface over a whole day may be similar across latitudes at times of maximum solar radiation, and that in comparison with other freshwater sources, photo-oxidation in the Rio Negro can be a significant source of atmospheric $CO_2$.

*4.1.2. Depth profiles and areal rates of photo-oxidation*

Photo-oxidation of DOC is a surface phenomenon due to its >50% dependence on UVB and UVA radiation, both of which are rapidly absorbed by the DOC in the top few cm (Granéli et al., 1998; Vähätalo et al., 2000). Indeed, in the present study, >60% of losses in absorbance were due to wavelengths ≤350 nm (Table 4). The depth over which photo-oxidation occurs will depend on the concentration and colour of the DOC as well as the concentration of other chemicals and particles in the water (e.g. Granéli et al., 1996; Vähätalo et al., 2000). Thus, it is important to characterize individual systems. In the present case, these data were important in visualizing the dynamics in the river and in delineating the depth range of areal photo-oxidation experiments. The majority of photo-oxidation and changes in absorbance indices occurred in the top 10 cm, and > 95% in the top 9 to 15 cm (Figs. 3, 4 and 10). These depth profiles are similar to those described by Vähätalo et al. (2000) in Lake Volkea-Kotinen (Finland, 12 mg $l^{-1}$ DOC) and by Granéli et al. (1996) in Lake Skärshultsjon (Sweden, 11.2 mg $l^{-1}$) for lakes of similar DOC content. However, DOC can lose colour or be of a lighter colour, increasing the depth of photo-oxidation as seen in Lake Sträken in Sweden, 9.2 mg $l^{-1}$ DOC (Granéli et al., 1996).

Areal rates of photo-oxidation were measured in two experiments, providing estimates of 28.8 and 39.3 mg C $m^{-2}$ $d^{-1}$ at average daily UV-R exposures of 58.7 and 61.7 mW $cm^{-2}$ $d^{-1}$, respectively. These are conservative estimates. Light shade covered the pool during dawn and dusk periods, leaving 7 h of full sunlight while the river would have received 12 h of full sunlight. Granéli et al., (1998) calculated that 75% of photo-oxidation occurred during the 6 h period around full noon in southern Swedish lakes. These data suggest that the decrease to the rates in the present study due to light shade and 7 h of direct sun exposure would be in the order of 10–15%. When applying the rates of photo-oxidation to the whole river, the rates may also be conservative if nearshore waters (used in the pool) had lower light transmission than offshore waters. This may have been the situation, particularly for experiment 7 (cf Section 3.4.2). In addition, as discussed above in 4.1.1, the rates of return of $CO_2$ to the atmosphere may be conservative as they did not include photo-oxidation of POC or production of CO.

The only other areal estimate of DOC photo-oxidation in the Rio Negro comes from the work of Remmington et al. (2011). They calculated that the annual average, daily rate of areal photo-oxidation of Rio Negro DOC was 24 mg C $m^{-2}$ $d^{-1}$ (200 nm $cm^{-2}$ $d^{-1}$). They considered this estimate conservative due to experimental limitations and the many assumptions they had to apply in their calculations. The present study improves on their estimate in directly measuring rates of photo-oxidation with depth in order to calculate areal photo-oxidation, and in recording simultaneous measures of UV-R exposure and temperature. Thus, our September–October estimates of photo-oxidation can form the basis of a more extensive data set to model annual patterns of photo-oxidation in the Rio Negro. The literature on seasonal changes in DOC quality and photo-oxidation (Lindell et al. (2000), Suhett et al. (2007), Rodrigues-Zuniga et al., 2008; Porcal et al. (2013a) and Holland et al. (2017), amongst others) indicate that a seasonal study of DOC characteristics and rates of photo-oxidation is required to better understand the roles of DOC in carbon cycling in the Rio Negro ecosystem.

Light intensity is a key variable controlling daily rates of areal photo-oxidation; consequently, rates in the tropics are not likely the highest in the world. Although all regions of the globe receive the same number of daylight hours during a year, their distribution changes with latitude. The higher is the latitude, the longer are the summer days, increasing the potential for high rates of daily photo-oxidation of DOC. The highest rates of areal photo-oxidation come from the Arctic during summer (35.8–296.4 mg C $m^{-2}$ $d^{-1}$) (Cory et al., 2014), followed by southern Swedish lakes with rates similar to the lower rates in the Arctic (44.3–171.1 mg C $m^{-2}$ $d^{-1}$) (Granéli et al., 1996). In September in The Netherlands, an areal photo-oxidation rate of 22 mg C $m^{-2}$ $d^{-1}$ was measured in a peaty lake (De Haan, 1993). The rate in The Netherlands under 12 h of sunlight was lower than in the tropics (present study) also under 12 h of sunlight. The solar cycle will tend to smooth out seasonal difference across the year across latitudes.

Annual rates of photo-oxidation are secondarily controlled by seasonal patterns of precipitation which control the seasonal pattern of light exposure and indirectly, the quality of DOC (e.g. Vähätalo et al., 2000; Porcal et al., 2013a). In the north-west of the Amazon Basin where the Rio Negro is situated, the wet season starts in December and extends until May, although rain occurs throughout the year (Espinoza Villar et al., 2009). In order to assess the impact of cloud cover during the rainy season on rates of DOC photo-oxidation, we extended the relationship between UV-R and near-surface rates of photo-oxidation (DOC = 10.8 mg $l^{-1}$) (Fig. 9) to the lower UV-R levels experienced in the 2015 November–December period (Table 1). Predicted daily rates of near-surface photo-oxidation ranged from 0.02 to 0.25 mg C $l^{-1}$ $d^{-1}$ in December compared with 0.46 and 0.50 mg C $l^{-1}$ $d^{-1}$ in November and values of 0.39 to 0.68 mg C $l^{-1}$ $d^{-1}$ in September–October 2018. This comparison assumes no change in DOC concentration or quality and that the relationship between rates of photo-oxidation and light is maintained in lower light levels. We did note that changes in absorbance still occurred, although at a reduced rate at the lowest UV-R (30.8 mW $cm^2$ $d^{-1}$) (Fig. 5). Thus, complete photo-oxidation of DOC could be nearly extinguished during periods of the rainy season. The December photo-oxidation rates might slightly underestimate $CO_2$ production because UV-R, particularly UVB, is removed more effectively by clouds than is PAR radiation which also contributes to photo-oxidation (Granéli et al., 1998). Considering the impact of the rainy season on photo-oxidation and the fact that areal rates of photo-oxidation vary less than concentrations of DOC (Granéli et al., 1996), it may be that large rivers in tropical rain forests have less annual $CO_2$ release back to the atmosphere from photo-oxidation per unit area than regions at higher latitudes which receive weaker sunlight (due to the greater distance light must travel through the atmosphere) but little summer cloud cover.

*4.2. Partial photo-oxidation at depth*

Losses in HA fluorescence, at all excitation wavelengths, extended 10 to 25 cm further down into the water column than losses of absorbance indices or of complete photo-oxidation. These observations were novel. Terrestrially derived fluorophores are quinone/semiquinone molecules (Cory and McKnight, 2005). On photo-oxidation, quinone/semiquinone molecules can produce singlet oxygen, a reactive oxygen species (ROS) which rapidly degrades to more destructive forms of ROS, such as the hydroxyl radical. Therefore, loss in HA fluorescence can be associated with changes to DOC structure due to ROS, including damage to the quinone/semiquinone group. Quinone molecules also act as redox systems giving or receiving electrons. In the more oxidized state their fluorescence is less intense and would be recorded as a loss. Therefore, loss of fluorescence may also represent a shift to a more oxidized state. Shift in redox state will alter how the DOC interacts with dissolved metal

ions. Thus, changes in fluorescence indicate changes in DOC structure and may include changes in average quinone/semiquinone redox state (Patel-Sorrentino et al., 2004; Cory and McKnight, 2005; Rodríguez-Zúñiga et al., 2008).

Does loss of deeper fluorescence mean more available DOC for microorganisms? Will it shift microbial composition? Others have shown that photo-oxidation can provide more-consumable DOC to the microbial community, particularly in humic systems (Amado et al., 2007; Lapierre and del Giorgio, 2014). Therefore, the loss of fluorescence may indicate some increase in consumable DOC in the water surface layer. Ward et al.'s (2017) studies indicate that the microbial community tends to evolve to consume the DOC that is present. The Rio Negro is a deep, fast flowing river which can stratify in periods of calm. It has also been observed to be well mixed to depth (Johannsson et al., 2017). It is unlikely that changes in the DOC composition in the surface layer can significantly alter the DOC structure available for most bacteria or for a long period of time. Bacteria in the Rio Negro grow better on the larger size fraction of the DOC (Amon and Benner, 1996b). This result suggests that photo-oxidation in the Rio Negro does little to alter the microbial community.

### 4.3. Conclusions

The most observable forms of photo-oxidation, the loss of absorbance and $CO_2$, occurred in the surface layer of the river, the top 9 to 15 cm. Yet we provide evidence of changes in DOC to more than double that depth associated with loss of fluorescence of humic-like substances. This is a novel finding. Fluorescence changes may have locally important consequence in increasing DOC available for bacterial consumption, for DOC susceptibility to future photo-oxidation, and for metal binding.

Areal rates of photo-oxidation, determined at the peak of seasonal sunlight were 28.8 and 39.3 mg C $m^{-2}$ $d^{-1}$: DOC was 10.8 mg $l^{-1}$. These rates are conservative, but provide quantitative values determined under as natural conditions as possible. Our study also quantified the relationship between UV radiation and near surface rates of photo-oxidation. Photo-oxidation estimates based on UV-R exposure in September–October and November–December revealed a strong seasonal precipitation/cloud cover pattern that controls the annual rate of photo-oxidation.

Climate change may modify the seasonal cycle. Inter-annual variability in precipitation will become higher and 'periods of wetness' more frequent (Duffy et al., 2015). Annual precipitation will increase in the headwater region and decrease near the mouth of the Rio Negro. We predict that stronger precipitation events with either reduced or no change in annual precipitation will lead to more hours of sunshine and higher rates of annual photo-oxidation of DOC for the majority of the river.

There are a number of knowledge gaps which need to be addressed before a seasonal model of photo-oxidation for the Rio Negro can be constructed. These include seasonal patterns in light and surface water temperature, as well as, photo-oxidation responses to low oxygen, higher temperatures and pH. Other important knowledge gaps are the seasonal variation in concentration and susceptibility of DOC to photo-oxidation, and the relationship between DOC concentration and rates of areal photo-oxidation.

## CRediT authorship contribution statement

**Ora E. Johannsson:** Conceptualization, Methodology, Investigation, Formal analysis, Writing - original draft, Visualization, Project administration. **Marcio S. Ferreira:** Methodology, Investigation, Formal analysis, Writing - review & editing. **D. Scott Smith:** Writing - review & editing, Investigation. **Anne Crémazy:** Investigation, Writing - review & editing. **Chris M. Wood:** Conceptualization, Funding acquisition, Resources, Methodology, Writing - review & editing. **Adalberto L. Val:** Conceptualization, Funding acquisition, Resources, Writing - review & editing, Project administration.

## Declaration of competing interest

The authors declare that they have no known competing financial interests or personal relationships that could have appeared to influence the work reported in this paper.

## Acknowledgements

Special thanks to personnel at INPA - Maria de Nazaré de Paula da Silva for her overall assistance, Rogério Santos Pereira for help and training on the DOC analyzer, and Réginaldo Oliveira and Thiago Nacimento for assistance with water collection and machinery. Thanks to Greg Goss of the University of Alberta for the loan of his Radiometer light meter, to Wallace Costa of INPA for the loan of his LiCor L-1000 data logger and quantum sensor, and to Raphael Duarte for sharing his absorbance and water quality information for the Rio Negro. We also recognize the constructive suggestions of three reviewers. Funding support in Brazil was from FAPEAM (062.01187/2017), CNPq (465540/2014-7) and CAPES (Financial Code 001) through an INCT-ADAPTA grant to ALV and a Ciência sem Fronteiras grant to ALV and CMW, and in Canada by the Natural Sciences and Engineering Research Council of Canada (NSERC) Discovery grants to CMW (RGPIN-2017-03843, RGPIN/473-2012) and DSS (RGPIN-2015-04414). MSF is the recipient of a Post-Doctoral fellowship from the Brazilian Centre for Improvement of Higher Education Personnel (Coordenação de Aperfeicoamento de Pessoal de Nıvel Superior, CAPES). ALV received a Research Fellowship from CNPq (303930/2014-4).

## Appendix A. Supplementary data

Supplementary data to this article can be found online at https://doi.org/10.1016/j.scitotenv.2020.139193.

## References

Alho, C.J.R., Reis, R.E., Aquino, P.P.U., 2015. Amazonian freshwater habitats experiencing environmental and socioeconomic threats affecting subsistence fisheries. Ambio 44, 412–425.

Al-Reasi, H.A., Wood, C.M., Smith, D.S., 2011. Physicochemical and spectroscopic properties of natural organic matter (NOM) from various sources and implications for ameliorative effects on metal toxicity to aquatic biota. Aquat. Toxicol. 103, 179–190.

Al-Reasi, H.A., Smith, D.S., Wood, C.M., 2012. Evaluating the ameliorative effect of natural dissolved organic matter (DOM) quality on copper toxicity to *Daphnia magna*: improving the BLM. Ecotoxicology 21, 525–537.

Amado, A.M., Cotner, J.B., Suhett, A.L., de Assis Esteves, F., Bozelli, R.L., Farjalla, V.F., 2007. Contrasting interactions mediate dissolved organic matter decomposition in tropical aquatic ecosystems. Aquat. Microb. Ecol. 49, 25–34.

Amon, R.M.W., Benner, R., 1996a. Photochemical and microbial consumption of dissolved organic carbon and dissolved oxygen in the Amazon River system. Geochim. Cosmochim. Acta 60, 1783–1792.

Amon, R.M.W., Benner, R., 1996b. Bacterial utilization of different size classes of dissolved organic matter. Limnol. Oceanogr. 41, 41–51.

Anesio, A.M., Granéli, W., 2003. Increased photoreactivity of DOC by acidification: implications for the carbon cycle in humic lakes. Limnol. Oceanogr. 48, 735–744.

Beltrão, H., Zuanon, J., Ferreira, E., 2019. Checklist of the ichthyofauna of the Rio Negro basin in the Brazilian Amazon. ZooKeys 881, 53–89.

Cole, J.J., Prairie, Y.T., Caraco, N.F., McDowell, W.H., Tranvik, L.J., Striegl, R.G., Duarte, C.M., Kortelainen, P., Downing, J.A., Middelburg, J.J., Melack, J., 2007. Plumbing the global carbon cycle: integrating inland waters into the terrestrial carbon budget. Ecosystems 10, 172–185.

Cory, R.M., McKnight, D.M., 2005. Fluorescence spectroscopy reveals ubiquitous presence of oxidized and reduced quinones in dissolved organic matter. Environ. Sci. Technol. 39, 8142–8149.

Cory, R.M., Ward, C.P., Crump, B.C., Kling, G.W., 2014. Sunlight controls water column processing of carbon in arctic fresh waters. Science 345, 925–928.

Crémazy, A., Wood, C.M., Smith, D.S., Ferreira, M.S., Johannsson, O.E., Giacomin, M., Val, A.L., 2016. Investigating copper toxicity in the tropical fish cardinal tetra (*Paracheirodon axelrodi*) in natural Amazonian waters: measurements, modeling, and reality. Aquat. Toxicol. 180, 353–363.

Dahlén, J., Bertilsson, S., Petterson, C., 1996. Effects of UV-A irradiation on dissolved organic matter in humic surface waters. Environ. Int. 22, 501–506.

De Haan, H., 1993. Solar UV-light penetration and photo-degradation of humic substances in peaty lake water. Limnol. Oceanogr. 38, 1072–1076.
DePalma, G.S.S., Arnold, W.R., McGeer, J.C., Dixon, D.G., Smith, D.S., 2011. Variability in dissolved organic matter fluorescence and reduced sulfur concentration in coastal marine and estuarine environments. Appl. Geochem. 26, 394–404.
Dias, D.A., Ghiggino, K.P., Smith, T.A., Scollary, G.R., 2010. Wine Bottle Colour and Oxidative Spoilage. Final Report to Grape and Wine Research and Development Corporation. School of Health and Biomedical Sciences, RMIT University, Melbourne, Australia.
Duffy, P.B., Brando, P., Asner, G.P., Field, C.B., 2015. Projections of future meteorological drought and wet periods in the Amazon. Proc. Natl. Acad. Sci. 112, 13172–13177.
Ertel, J.R., Hedges, J.I., Devol, A.H., Richey, J.E., Ribeiro, M.N.G., 1986. Dissolved humic substances in the Amazon River system. Limnol. Oceanogr. 31, 739–754.
Espinoza Villar, C.J., Ronchail, J., Guyot, J.L., Cochonneau, G., Naziano, F., Lavado, W., De Oliveira, E., Pombosa, R., Vauchel, P., 2009. Spatiotemporal rainfall variability in the Amazon basin countries (Brazil, Peru, Bolivia, Columbia, and Ecuador). Int. J. Climatol. 29, 1574–1594.
Evans, C.D., Futter, M.N., Moldan, F., Valinia, S., Frogbrook, Z., Kothawala, D.N., 2017. Variability in organic carbon reactivity across lake residence time and trophic gradients. Nat. Geosci. 10, 832–835.
Granéli, W., Lindell, M., Tranvik, L., 1996. Photo-oxidative production of dissolved inorganic carbon in lakes of different humic content. Limnol. Oceanogr. 41, 698–706.
Granéli, W., Lindell, M., de Faria, B.M., Esteves, F., 1998. Photo-production of dissolved inorganic carbon in temperate and tropical lakes – dependence on wavelength band and dissolved organic carbon concentration. Biogeochemistry 43, 175–195.
Holland, A., Wood, C.M., Smith, D.S., Correia, T.G., Val, A.L., 2017. Nickel toxicity to cardinal tetra (*Paracheirodon axelrodi*) differs seasonally and among the black, white and clear river waters of the Amazon basin. Water Res. 123, 21–29.
Johannsson, O.E., Smith, D.S., Sadauskas-Henrique, H., Cimprich, G., Wood, C.M., Val, A.L., 2017. Photo-oxidation processes, properties of DOC, reactive oxygen species (ROS), and their potential impacts on native biota and carbon cycling in the Rio Negro (Amazonia, Brazil). Hydrobiologia 789, 7–29.
Koehler, B., Landelius, T., Weyhenmeyer, G.A., Machida, N., Tranvik, L.J., 2014. Sunlight-induced carbon dioxide emissions from inland waters. Glob. Biogeochem. Cycles 28, 696–711. https://doi.org/10.1002/2014GB004850.
Küchler, I.L., Forsberg, B.R., 2000. A contribution to the chemical characterization of Rivers in the Rio Negro basin, Brazil. J. Braz. Chem. Soc. 11, 286–292.
Lapierre, J.F., del Giorgio, P.A., 2014. Partial coupling and differential regulation of biologically and photo-chemically labile dissolved organic carbon across boreal aquatic networks. Biogeosciences 11, 5969–5985.
Latrubesse, E.M., Franzinelle, E., 2005. The late Quaternary evolution of the Negro River, Amazon, Brazil: implications for island and floodplain formation in large anabranching tropical systems. Geomorphology 70, 372–397.
Lindell, M.J., Granéli, H.W., Bertilsson, S., 2000. Seasonal photo-reactivity of dissolved organic matter from lakes with contrasting humic content. Can. J. Fish. Aquat. Sci. 57, 875–885.
McKnight, D.M., Boyer, E.W., Westerhoff, P.K., Doran, P.T., Kulbe, T., Anderson, D.T., 2001. Spectrofluorometric characterization of dissolved organic matter for indication of precursor organic material and aromaticity. Limnol. Oceanogr. 46, 38–48.
Molot, L.A., Dillon, P.J., 1997. Photolytic regulation of dissolved organic carbon in northern lakes. Glob. Biogeochem. Cycles 11, 357–365.
Molot, L.A., Hudson, J.J., Dillon, P.J., Miller, S.A., 2005. Effect of pH on photo-oxidation of dissolved organic carbon by hydroxyl radicals in a coloured, soft-water stream. Aquat. Sci. 67, 189–195.
Patel-Sorrentino, N., Mounier, S., Luca, Y., Benaim, J.Y., 2004. Effects of UV–visible irradiation on natural organic matter from the Amazon basin. Sci. Total Environ. 321, 231–239.
Porcal, P., Dillion, P.J., Molot, L.A., 2013a. Seasonal changes in photochemical properties of dissolved organic matter in small boreal streams. Biogeosciences 10, 5533–5543.
Porcal, P., Dillon, P.J., Molot, L.A., 2013b. Photo-chemical production and decomposition of particulate organic carbon in a freshwater stream. Aquat. Sci. 75, 469–482.
Porcal, P., Dillion, P.J., Molot, L.A., 2015. Temperature dependence of photo-degradation of dissolved organic matter to dissolved inorganic carbon and particulate organic carbon. PLoS One 10 (6), e0128884.
Raymond, P.A., Hartmann, J., Lauerwald, R., Sobek, S., McDonald, C., Hoover, M., Butman, D., Striegl, R., Mayorga, E., Humborg, C., Kortelainen, P., Dürr, H., Meybeck, M., Ciais, P., Guth, P., 2013. Global carbon dioxide emissions from inland waters. Nature 503, 355–359.
Remmington, S., Krusche, A., Richey, J., 2011. Effects of DOM photochemistry on bacterial metabolism and $CO_2$ evasion during falling water in a humic and a whitewater river in the Brazilian Amazon. Biogeochemistry 105, 185–200.
Richey, J.E., Melack, J.M., Aufdenkampe, A.K., Ballester, V.M., Hess, L.L., 2002. Outgassing from Amazonian rivers and wetlands as a large tropical source of atmospheric $CO_2$. Nature 147, 617–620.
Rodríguez-Zúñiga, U.F., Pereira Milori, D.M.B., Lopes da Silva, W.T., Martin-Neto, L., Camargo Oliveira, L., Rocha, J.C., 2008. Changes in optical properties caused by UV-irradiation of aquatic humic substances from the Amazon River basin: seasonal variability evaluation. Environ. Sci. Technol. 42, 1948–1953.
Scully, N.M., McQueen, D.J., Lean, D.R.S., Cooper, W.J., 1996. Hydrogen peroxide formation: the interaction of ultraviolet radiation and dissolved organic carbon in lake waters along a 43–75_N gradient. Limnol. Oceanogr. 41, 540–548.
Suhett, A.L., Amado, A.M., Enrique-Prast, A., de Assis Esteves, F., Farjalla, V.F., 2007. Seasonal changes in dissolved organic carbon photo-oxidation rates in a tropical humic lagoon: the role of rainfall as a major regulator. Can. J. Fish. Aquat. Sci. 64, 1266–1272.
Thurman, E.M., 1985. Organic Geochemistry of Natural Waters. Martinus Nijhoff./Dr. W. Junk Publishers, Dordrecht.
Vähätalo, A.V., Salkinoja-Salonen, M., Taalas, P., Salonen, K., 2000. Spectrum of the quantum yield for photochemical mineralization of dissolved organic carbon in a humic lake. Limnol. Oceanogr. 45, 664–676.
Val, A.L., Almeida Val, V.M.F., 1995. Fishes of the Amazon and their environment, physiological and biochemical aspects. In: Bradshaw, S.D., Burggren, W., Heller, H.C., Ishii, S., Langer, H., Neuweiler, G., Randall, D.J. (Eds.), Zoophysiology. 32. Springer-Verlag, Berlin, Germany, p. 221.
Ward, C.P., Nalven, S.G., Crump, B.C., Kling, G.W., Cory, R.M., 2017. Photochemical alteration of organic carbon draining permafrost soils shifts metabolic pathways and stimulates respiration. Nat. Commun. 8, 1–8.
Wetzel, R.G., 1975. Limnology. 19105. W.B. Saunders Co, Philadelphia, PA, USA, p. 743.
Wood, C.M., Al-Reasi, H.A., Smith, D.S., 2011. The two faces of DOC. Aquat. Toxicol. 105S, 3–8.
www.physics.uoguelph.ca/~pgarrett/Teaching.html. Physics teaching help. Accessed latest March 15, 2016. (http://www.technicalglass.com/fused_quartz_transmission.html), Accessed latest November 15 2019.